

FEATURE ARTICLE

Synaptic Properties of Connections between the Primary and Secondary Auditory Cortices in Mice

Elise N. Covic and S. Murray Sherman

Department of Neurobiology, University of Chicago, Chicago, IL 60637, USA

Address correspondence to Elise N. Covic, Northwestern University, Morton Building 1-670, 303 East Chicago Avenue, Chicago, IL 60611, USA.
Email: e-covic@northwestern.edu.

Little is known regarding the synaptic properties of corticocortical connections from one cortical area to another. To expand on this knowledge, we assessed the synaptic properties of excitatory projections from the primary to secondary auditory cortex and vice versa. We identified 2 types of postsynaptic responses. The first class of responses have larger initial excitatory postsynaptic potentials (EPSPs), exhibit paired-pulse depression, are limited to ionotropic glutamate receptor activation, and have larger synaptic terminals; the second has smaller initial EPSPs, paired-pulse facilitation, metabotropic glutamate receptor activation, and smaller synaptic terminals. These responses are similar to the driver and modulator properties previously identified for thalamic and thalamocortical circuitry, suggesting that the same classification may extend to corticocortical inputs and have an implication for the functional organization of corticocortical circuits.

Keywords: auditory cortex, cortical connectivity, corticocortical inputs, glutamate, laser uncaging of glutamate

Introduction

The functional properties of connections between cortical areas are poorly understood. Three related issues restrict this understanding. First, data available to address this issue have been dominated by studies that are anatomical in nature (Zeki 1970, 1974, 1976, 1980; Zeki and Sandeman 1976; Seltzer and Pandya 1978; Rockland and Pandya 1979; Maunsell and van Essen 1983; Miller 1985; Shipp and Zeki 1985, 1989, 1995; Gilbert and Wiesel 1989; Zeki and Shipp 1989; Bravo et al. 1990; Coogan and Burkhalter 1990; Felleman and Van Essen 1991; Lowenstein and Somogyi 1991; Scannell et al. 1995; Kaas 1996; McDonald and Mascagni 1996; Porter 1997; Beck and Kaas 1998; Shipp et al. 1998; Kaas and Collins 2001; Wu and Kaas 2003; Kaskan and Kaas 2007; Wong and Kaas 2009) with surprisingly little functional information about these connections. Thus, we lack a basic understanding of how these circuits actually function. Implicit in various interpretations of the anatomical data is the notion that the main avenues of communication are glutamatergic, excitatory, functionally homogeneous, and operate to support corticocortical processing in a sort of anatomical democracy, where functional strength and relevance are determined by the number of inputs (Zeki 1974; Rockland and Pandya 1979; Stone et al. 1979; Maunsell and van Essen 1983; Shipp and Zeki 1989; Coogan and Burkhalter 1990, 1993; Felleman and Van Essen 1991; Lowenstein and Somogyi 1991; Kaas 1996; Kaas and Collins 2001). This raises the second issue, namely, whether the excitatory glutamatergic inputs are functionally homogenous or can instead be classified into

distinct types. Such a classification, because it identifies functionally distinct inputs, would have obvious implications for understanding the functional organization of corticocortical connectivity. Third, most studies examining the physiological relationship of corticocortical connections, although informative, have often been limited to the examination of connections within a cortical area (Fleiderovich et al. 1998; Atzori et al. 2001; Frick et al. 2007), inhibitory influences (Reyes et al. 1998; Dong et al. 2004), recordings of large groups of summed neural responses (Domenici et al. 1995; Hishida et al. 2003), or recordings and/or stimulation sites involving single layers (Shao and Burkhalter 1996; Reyes et al. 1998). A systematic exploration of the corticocortical laminar origin and termination is necessary to understand the functional organization of excitatory cortical circuitry. Toward this end, we have used a mouse brain slice preparation to investigate synaptic properties in the pathways linking the first auditory cortical area (A1) and ventral region of the second (A2v) in both directions (Prieto et al. 1994; Ehret 1997).

Materials and Methods

Slice Preparation and Electrophysiological Recordings

We adopted our previously published techniques for this study, which are described elsewhere (Reichova and Sherman 2004; Lam and Sherman 2005; Llano and Sherman 2008; Lee and Sherman 2009a, 2009b). All procedures were approved by the Institutional Animal Care and Use Committee of the University of Chicago. Brain slices were taken from BALB/c mice aged 12–19 days postnatal. Whole-cell recordings were made in either A2v ($n = 91$) or A1 ($n = 72$) from visually identified neurons in layers 2/3 through 6. The mice were anesthetized with a few drops of isoflurane (AErrane, Baxter Pharmaceuticals) and decapitated. The brains were removed and placed in chilled (0 °C) artificial cerebrospinal fluid (ACSF). After blocking the brain, corticocortical slices (~400 μm thick) were cut coronally to include both A1 and A2v. The viability of connections between these areas was initially confirmed through bulk anatomical injections of neural tracer to ensure that fibers remained intact for our slice preparation. Before recording, slices were held in a chamber with ACSF for 1 h at room temperature (~25 °C). At all times, they were oxygenated with carbogen (5% CO_2 -95% O_2). For recording, slices were transferred to a submerged recording chamber and continually perfused with oxygenated ACSF at 32 °C. The ACSF composition was as follows (in mM): 125 NaCl, 25 NaHCO_3 , 3 KCl, 1.25 NaH_2PO_4 , 1 MgCl_2 , 2 CaCl_2 , and 25 glucose.

Recordings were limited to neurons with a stable access resistance of less than 20 M Ω . Electrodes were pulled from borosilicate glass (Garner Glass) with input resistances of ~6 to 10 M Ω after filling with the following intracellular solution (in mM): 135 KGlucuronate, 7 NaCl, 10 4-(2-hydroxyethyl)-1-piperazineethanesulfonic acid, 2 Na_2ATP , 0.3 Na_3GTP , 2 MgCl_2 , 0.5–1 mM dinitrostitilbene-2,2'-disulfonic acid (DNDS), and 0.1–0.5% biocytin. The pH of the solution was adjusted to 7.3 using KOH, and osmolality was adjusted to 290 mOsm with

distilled water. The use of this intracellular solution resulted in ~ 10 mV junction potential.

All recordings were made on a visualized rig with infrared differential interference contrast. Laminae were identified based on the following criteria: Layer 1 appeared thin and aneuronal; Layers 2 and 3 were not easily distinguishable and are considered below as “layers 2/3”; these sat directly above the dense packing of cells residing in layer 4. Layer 5a was easily distinguishable based on the sparse patterns of cell packing in comparison the layer 4. Layer 5b was evident due to an increased pattern of cell packing density that was greater than 5a but not as pronounced as layer 4. Layer 6 followed with a less densely populated layer than the previous (Lachica et al. 1992; Lachica and Casagrande 1992, 1993).

Recordings were made in either current clamp or voltage clamp, using a Multiclamp 700B amplifier and pClamp software (Axon Instruments; Walz 2007). To determine the laminar location of recorded cells, a normalized depth value for each cell was calculated using the distance from the pia to the patch electrode. This depth value was converted to a laminar location based on the published descriptions of the mouse auditory cortex (Caviness 1975; Cruikshank et al. 2001; Paxinos and Franklin 2001) and was used to complement the above-mentioned criteria; the 2 methods of laminar determination were in agreement. Laminar locations of recorded cells were further confirmed in selected experiments by filling patched neurons with biocytin. We identified neurons that appeared larger for patch recordings. The cells successfully filled with biocytin were types of excitatory spiny neurons—either pyramidal or stellate. In each case, the filled cells identified the laminar location of the cell body in addition to the morphology of the recorded cell. Once patched, we studied responses to injected current, both hyperpolarizing, to identify I_H , and depolarizing to identify regular, tonic, or bursting spike patterns.

To assess paired-pulse effects, it was essential to apply γ -aminobutyric acid (GABA)_A antagonists to isolate glutamatergic synapses (i.e., a build-up of postsynaptic GABA responses could make a facilitating glutamatergic response seem depressing). However, bath application of GABA_A antagonists, at concentrations necessary for the complete blockade of inhibition, often induce a hyperexcitable state, resulting in paroxysmal activity of the cortical slice. Thus a GABA_A antagonist, DNDS, was included in the recording electrode (Dudek and Friedlander 1996). DNDS is a chloride channel blocker used intracellularly to inhibit GABA_A-ergic inhibitory postsynaptic potentials; it diffuses into the postsynaptic cell from the intracellular recording electrode. Restricting the blockade of inhibition to a single neuron leaves only the presumed excitatory component of evoked postsynaptic potential and eliminates the problems of paroxysmal activity seen when GABA antagonists are added to the bath (Dudek and Friedlander 1996). To assess the reliability of DNDS as an intracellular GABA_A antagonist,

control experiments were done to see if the inhibitory response normally induced by the addition to the circulating bath of muscimol (10 μ M), a GABA_A agonist, would be abolished when DNDS was included in the intracellular solution. See Figure 1 for evidence of efficacy of DNDS in our experiments.

Uncaging of Glutamate

Inputs to the patched neuron were identified by monitoring EPSCs elicited by laser photostimulation (Lam and Sherman 2005) aided by the use of custom acquisition and analysis software written in Matlab (MathWorks, Inc.). Nitroindolyl-caged glutamate (Sigma-RBI; Canevari et al. 2001) was added to recirculating ACSF to a concentration of 0.37 mM. Once whole-cell recording was established, focal photolysis of caged glutamate was accomplished by Q-switching the pulsed UV laser (355 nm wavelength, frequency-tripled Nd:YVO₄, 100 kHz pulse repetition rate; DPSS Lasers, Inc.), to give a 1 ms, 100-pulse light stimulus. Stimulus intensities were controlled by neutral density filters and recorded with each stimulus presentation by a photodiode. A beam intensity of 5 mW was used. The laser beam position was controlled with mirror galvanometers (Cambridge Scanning, Inc.). The beam entered the microscope via a dichroic mirror and was focused using a low numerical aperture (NA) and low-magnification objective lens (10 \times /0.3 NA/water UPlanFl or 4 \times /0.13 NA/air UPlanFl; Olympus). Beam expansion was limited to a 2-fold gain through the scan lens/tube lens pair, yielding a narrow beam that greatly under-filled the objective and could therefore be focused on a spot in the specimen plane that was small in the x - y dimension (~ 10 μ m) but large in the z -axis (>100 μ m). Control experiments have shown that individual dendrites are directly stimulated by glutamate uncaging at a lateral (x - y) resolution of ~ 15 μ m (Lam and Sherman 2005). A computer controlled the stimulation of a preset grid in which all points were stimulated, but in a sequence designed to avoid problems related to short-term synaptic effects (e.g., receptor desensitization). Voltage traces were quantified by measuring the total area under the traces within 100 ms after UV stimulus onset, using custom software. The laser uncaging of glutamate only results in activation at the cell body or proximal dendrites and, therefore, avoids activating axons, either antidromically or axons of passage (Shepherd et al. 2003).

To localize the inputs to our patched cells in A1 or A2v, we targeted small regions of the presumed afferent area (A2v or A1, respectively) in a grid-like laminar-specific fashion for photostimulation with laser uncaging of glutamate while recording the target cell in voltage clamp. We thereby determined the area of input cortex containing afferent cells, an area we call the “footprint,” and we also determined the region evoking the largest responses, a region we call the hotspot; in all cases, the hotspot was near the center of the footprint.

Glutamatergic Synaptic Physiology

Concentric bipolar stimulating electrodes (FHC, 125 μ m pole distance) were centered on the hotspots elicited by photostimulation. A potential problem with extracellular stimulation is that axons of passage can be activated, as well as antidromic activation. To minimize this problem, synaptic responses were activated by minimal electrical stimulation; by “minimal electrical stimulation” we do not assume single axons were stimulated, but rather we used a protocol of just-above-threshold activation to minimize stimulating inappropriate axons, as axons have higher activation thresholds (Pan and Colbert 2001; Colbert and Pan 2002; Bhadra et al. 2007). We found the stimulation level that activated an EPSP 50% of the time and then used a 5–10% increase of that activation level for most other analyses. Increasing levels of electrical stimulation were then used to test for graded versus all-or-none responses by varying the intensity in 50 μ A increments until reaching 300 μ A of intensity for all recordings. Here, we simply plotted the amplitude of the evoked EPSP against the stimulation intensity. Stimulation consisted of 0.1–0.2 ms pulses from 10–130 Hz. Low-frequency stimulation readily activated ionotropic glutamate receptors (iGluRs), but a train of high-frequency (we typically used 130 Hz) stimulus was usually necessary to elicit a metabotropic GluR (mGluR) response (McCormick and von Krosigk 1992; Wu et al. 2001). Responses were considered monosynaptic if the latency jitter was less than 1 ms and had similar rise times between trials. The receptors that

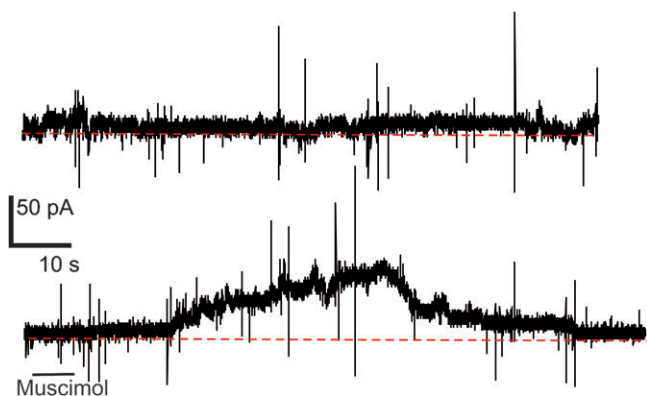


Figure 1. Control experiment to test the efficacy of intracellular DNDS application. The upper trace shows that muscimol has no effect on the cell when DNDS is in the intracellular solution. The lower trace shows the typical response to muscimol recorded in a nearby cell in the same slice without DNDS. In all 7 cases of such paired controls, the cells with normal intracellular solution responded to muscimol with inhibitory outward currents. Cells recorded with DNDS showed no response.

mediate the observed EPSPs were determined by comparing the responses in the presence of specific antagonists versus the control situation, where no antagonists were present. All experimental protocols were performed in the presence of DNDS. To isolate possible metabotropic responses, high-frequency stimulation was applied in the presence of NMDA and AMPA antagonists (MK-801 [40 μ M] and 6,7-dinitroquinoxaline-2,3-dione [50 μ M], respectively) in all recordings. Finally, the mGluR1 antagonist LY367385 (40 μ M), the mGluR5 antagonist MPEP (50 μ M), and the Group II mGluR antagonist MCCG (50 μ M) were used to block and identify various types of activated mGluRs. These agonists, antagonists, and concentrations were chosen based on their efficacy in characterizing corticothalamic and thalamocortical inputs in the mouse somatosensory and auditory systems (Reichova and Sherman 2004; Lee and Sherman 2009a, 2009b). Agonist and antagonist stock solutions were prepared in distilled water and diluted to their final concentration just before use. Pharmacological agents were bath applied through the use of a motorized stage pump. Based on the rate of injection and chamber perfusion, the final bath concentration was generally estimated to be one-fourth of the initial concentration. The bath application flowed for a minimum of 5 min before using any stimulation protocol. To eliminate synaptic activity in controls to determine whether evoked mGluR types were present postsynaptically, the general mGluR agonist, trans-(1S,3R)-1-Amino-1,3-dicarboxycyclopentane (ACPD) (TOCRIS) at 100 μ M, was applied to a preparation with a low-Ca²⁺ (0.2 mM)/high-Mg²⁺ (6 mM) ACSF solution combined with iGluR antagonists.

Anatomical Methods

Adult mice (60 days or older) were anesthetized with an intraperitoneal (IP) injection of ketamine hydrochloride (100 mg/kg) and xylazine (3 mg/kg) and then placed in a stereotaxic apparatus. (We note that these anatomical tracing experiments were done in fully adult mice, whereas the electrophysiology was done on juvenile mice, and this might somewhat obscure the correlations between anatomy and physiology seen in Results.) Aseptic conditions were maintained throughout the surgery. The animal's body temperature was kept at 37 °C using a thermal pad under feedback control. Response to toe pinch and blinking were monitored, and IP supplements of anesthesia were administered as needed. Small micropipettes (tip diameter 5–15 μ m) filled with a solution of biocytin (1–5%) or biotinylated dextran amine (BDA; molecular weight of 10 000, 2.5%—Vector Labs) were lowered into A1 or A2v orthogonally to the pial surface with the guidance of stereotaxic coordinates. The tracers were injected iontophoretically via positive current pulses of 5 μ A, 7 s duration, half duty cycle for 10–30 min. The animals were allowed to survive for 24–48 h and were then deeply anesthetized with an IP injection of pentobarbital (100 mg/kg) and perfused transcardially with 4% paraformaldehyde in phosphate-buffered saline (PBS). Areas of interest were blocked, post-fixed overnight in a fixative perfusate, and then sectioned coronally on a sliding microtome at 50 μ m. A peroxidase (Vectastain Elite ABC-Peroxidase Kit, Vector Labs), nickel/cobalt intensified, diaminobenzidine reaction was performed. Light level images of the injection sites and labeled areas in A1 or A2v were taken with a Zeiss Axiocam digital camera. Identical methods were used to identify laminar locations of neurons filled with biocytin during recordings (Llano and Sherman 2008).

For immunostaining with an antibody to mGluR2 (a Group II mGluR), selected sections were pretreated for 30 min in 0.5% H₂O₂, rinsed in PBS then incubated for 2 h in PBS containing 0.3% Triton X-100. Areas of interest were then blocked using an Avidin/Biotin Blocking Kit (Vector Labs), followed by immersion in 2% normal rabbit serum for 2 h (NRS; Vector Labs) were then incubated at 4 °C for 12–48 h in a primary antibody solution. PBS was used for all rinses, except the final rinse, which utilized Tris-buffered saline (TBS, 0.01 M, pH 8). Following rinses in TBS and PBS, sections were mounted on gelatin-coated slides, air dried, dehydrated with increasing concentrations of alcohol, cleared with xylene, and cover slipped using Permount (Fisher; Lee and Sherman 2009a, 2009b).

The areas of synaptic terminals labeled in A2v from the A1 (or A1 from A2v) injections were assessed with the use of Axiocam digital camera software and a digitizing mouse stylus tablet (Wacom). Images of obvious terminals were taken from the same area but at varying depths throughout the 50 μ m-thick histological section. With the use

of Image-J software, all images representing different 3D values were added together to produce one 2D image. A 1600 × 1400 pixel area of each image was overlaid with a grid and was then assessed. To minimize sampling biases, we started in the upper left-hand corner over the overlaid grid and measured the area of every detected terminal in the corner box of the grid. We continued to measure terminals in all boxes of the grid, moving row by row until 100-labeled terminals were measured. Resampling was not an issue since the Axiocam software leaves previous measurement traces on screen. For each section with obvious terminal fields ending in A2v ($n = 10$), Layers 5a, 5b, and 6 were analyzed by tracing the perimeter of each terminal. The Axiocam software then calculates the area inside of the trace. In each of the 3 layers noted from A2v (layers 5a, 5b, and 6), 100 terminals were measured for each of 10 samples, giving us 3000-labeled synaptic terminals from the 3 layers. Since we were testing the hypothesis that the different Classes of input would correlate with terminal size in both directions, layers receiving a mix of input types were excluded from analysis, and thus, we concentrated on layers receiving a pure, or nearly pure, input of a single Class. For analysis of terminal fields in A1 ($n = 5$), layers 4, 5a, 5b, and 6 were analyzed. In each of the 4 layers noted from A1 (layers 4, 5a, 5b, and 6), 100 terminals were measured per each of the 5 samples, giving us 2000-labeled synaptic terminals. Similar methodology for measuring terminal size can be found in Llano and Sherman (2008).

Results

Identification of Auditory Cortical Areas

Figure 2 shows a differential interference contrast (DIC) image of live auditory cortical tissue taken just prior to a recording session. Compared with A2v, A1 has increased cell-packing densities and better-defined laminar organization. Coronal sections immunostained with a Group II mGluR antibody further support these patterns (Fig. 2B,C). In addition, A1 exhibits a greater granular appearance in comparison to A2v. To confirm the locations of A1 and A2v, we injected biocytin, which transports both anterogradely and retrogradely, in A1 in vivo to demonstrate that orthograde labeling was found in A2v and retrograde labeling in the thalamic afferent nucleus, MGBv. Figure 2D reveals the injection site in A1 as well as the labeled terminal field in area A2v. Figure 2E, which shows another slice from the same brain, reveals a terminal field in A2v as well as retrograde labeling in MGBv.

Layers were identified based on the following criteria: Layer 1 appeared thin and aneuronal; Layers 2/3 were not easily distinguishable and sat directly above the dense packing of cells residing in layer 4. Layer 5a was distinguishable based on the sparse patterns of cell packing in comparison to layer 4. Layer 5b was evident due to an increased pattern of cell packing density that was greater than layer 5a but not as pronounced as layer 4. Layer 6 had a lower packing density than layer 5b.

The A1 to A2v Pathway

Whole-cell recordings were obtained from 91 neurons in layers 2/3, 4, 5a, 5b, and 6 of A2v in response to stimulation of A1. The cells had resting membrane potentials of -62.8 ± 3.7 mV and input resistances of 359.2 ± 126.4 M Ω .

Glutamatergic Response Classes

In order to assess possible differences in glutamatergic response Classes, the corticocortical synapses were initially activated by using laser uncaging of glutamate (i.e., photostimulation; Callaway and Katz 1993; Lam and Sherman 2005). A stimulating electrode was then placed on the afferent region, which was

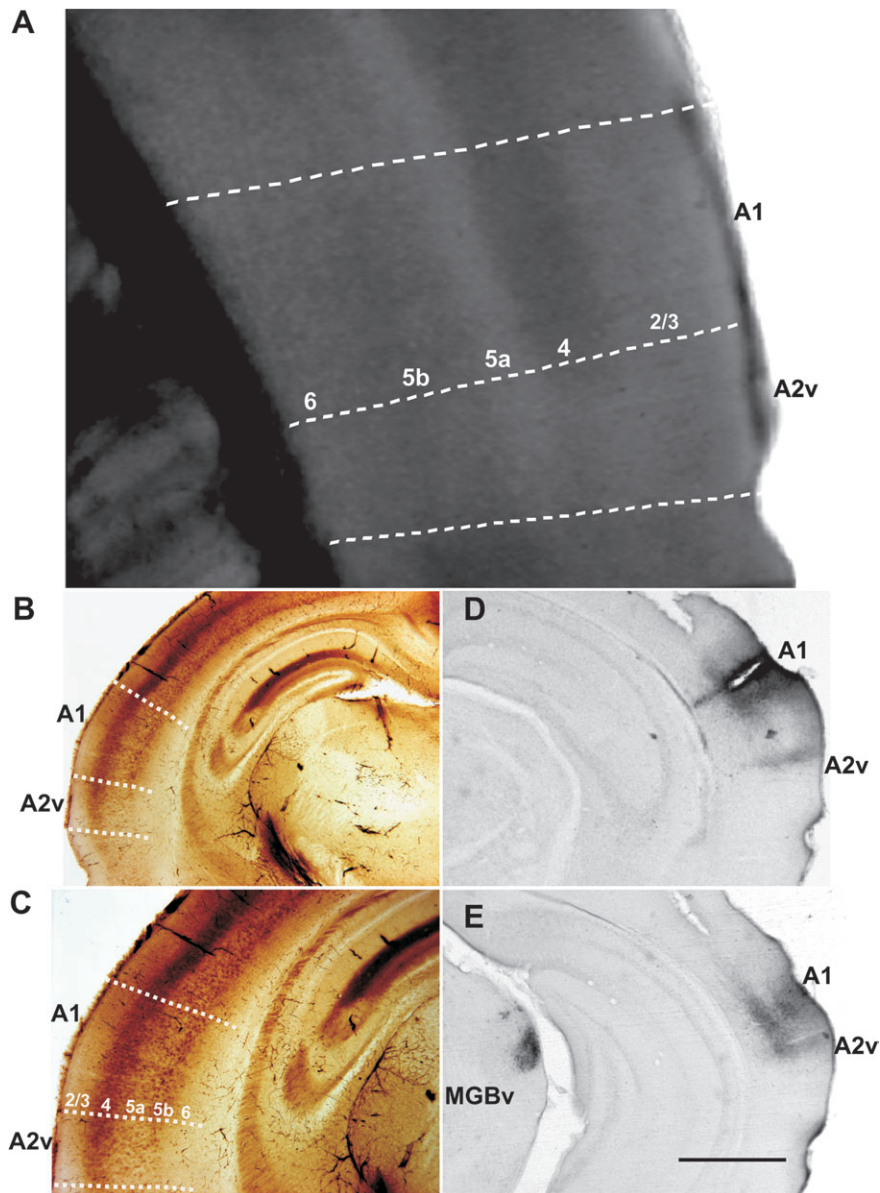


Figure 2. (A) DIC image of living slice just prior to recording. Area A1 has increased cell packing densities as well as better-defined laminar organization compared with A2v. (B,C) Image of slice similar to that in A immunostained with a Group II mGluR antibody. (D,E) Example of a biocytin injection into A1, showing the site (D) and labeled terminal field in A2v (D,E). Labeling is also seen in the MGBv (E). The scale bar in E is 0.2 mm for A, 1 mm for B, D, and E, and 0.5 mm for C.

determined by photostimulation to be the region that yielded the strongest response (i.e., the hotspot) in order to test for various synaptic properties. We noted 2 different response profiles, which we refer to initially as “Class 1B” and “Class 2.” The unusual terminology for Class 1B stems from a recent report of classification of thalamocortical inputs describing 2 classes, which were termed Class 1 and Class 2 (Viaene et al. 2011). Our Class 2 appears to have the same properties as their Class 2. However, our Class 1B is very similar but not identical to their Class 1, and as we explain in Discussion, we are not clear as to whether our Class 1B is truly a different Class, and so we have at least temporarily hedged our bets by renaming the original Class 1 as “Class 1A” and that seen here as “Class 1B.”

Figure 3A–D shows an example of a Class 1B response for a cell recorded in layer 5b of A2v and activated from layer 4 of A1 (Fig. 3A). Electrical stimulation elicited paired-pulse de-

pression when stimulated at a rate of 10–20 Hz (Fig. 3B), with an initial large amplitude EPSP followed by EPSPs of progressively smaller amplitudes. At 10–20 Hz, EPSPs were blocked by iGluR antagonists (Fig. 3C). Further attempts to activate a response at high stimulus frequency, which is often needed to activate mGluRs (McCormick and von Krosigk 1992; Wu et al. 2001), produced no evidence of any mGluR response component (Fig. 3D).

A Class 2 response is illustrated in Figure 3E–H for a cell recorded in layer 5a of A2v while stimulating in layers 2/3 of A1 (Fig. 3E). While stimulated at 15 Hz, this neuron exhibited paired-pulse facilitation with evoked EPSPs that started small but became progressively larger in amplitude (Fig. 3F). Antagonists to iGluRs blocked EPSPs activated at 15 Hz (Fig. 3G), but high-frequency stimulation evoked a sustained slow change in membrane potential (Fig. 3H) corresponding to an mGluR

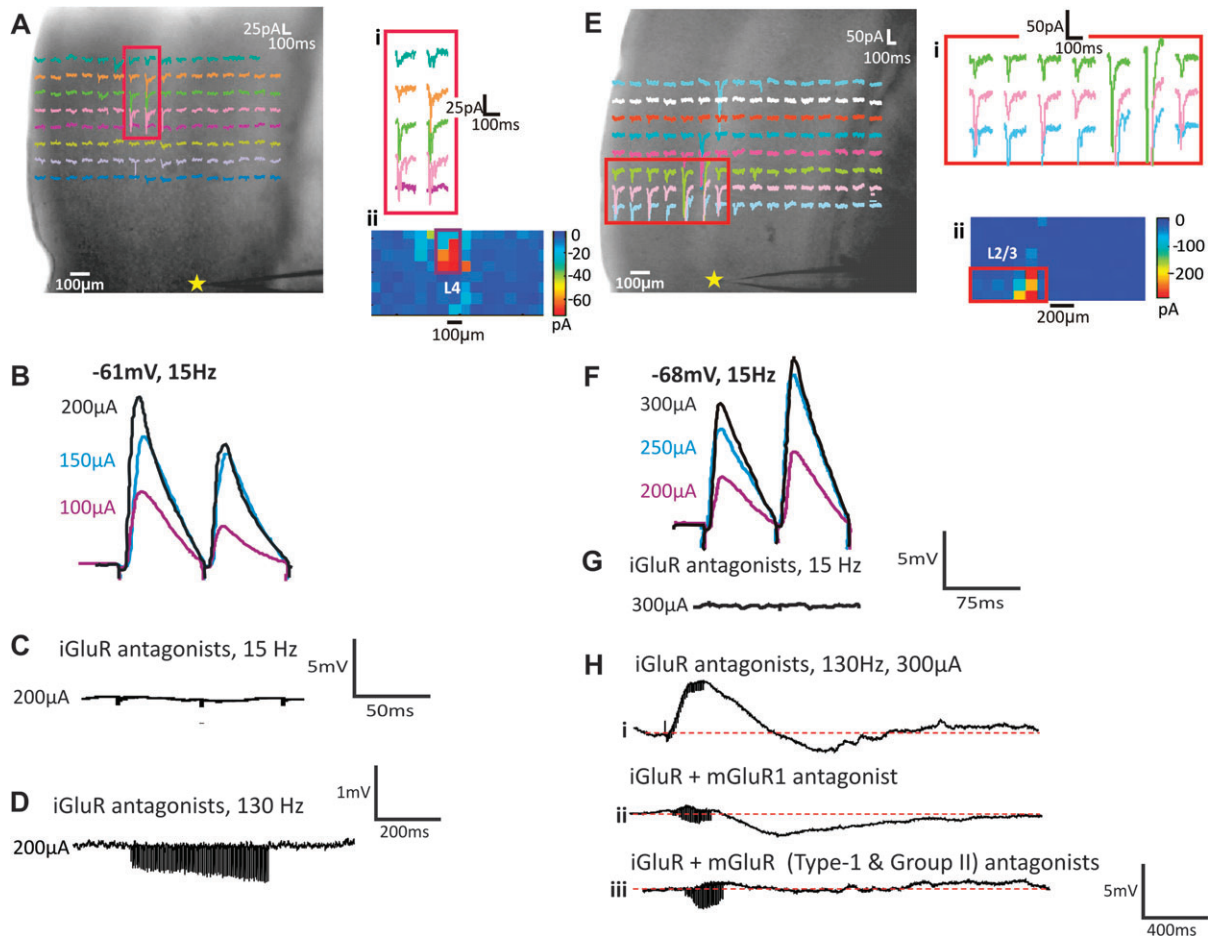


Figure 3. Response examples. (A–D) Class 1B response for cell in layer 5b of A2v (star in A) with activation hotspot in layer 4 of A1. Responses enlarged in A, and in false color in A_{ii}. Electrical stimulation of hotspot shows paired-pulse depression (B) with responses blocked by iGluR antagonists (C) even at and high stimulation rates (D). (E–H) Class 2 response for cell recorded in layer 5a of A2v; conventions as in A–D. Here, we see paired-pulse facilitation (F) and depolarizing/hyperpolarizing mGluR activation (H_i); the depolarizing component is blocked by an mGluR1 antagonist (H_{ii}) and the hyperpolarizing component by a Group II antagonist (H_{iii}).

response. Interestingly, this mGluR response included a mixture of both an excitatory component (Group I mGluR activation; Fig. 3_i) plus an inhibitory component (Group II mGluR activation; Fig. 3H_{ii}). Such inhibitory Group II responses have been previously reported in cortex (Lee and Sherman 2009a, 2009b). Class 2 responses always exhibited mGluR response components, either Group I, Group II, or as in the illustrated example, both.

Because of the time course of evoked mGluR responses, we could not use latency measures to determine whether these were activated monosynaptically or via intermediary cortical circuitry. Given that all iGluRs were blocked during high-frequency stimulation trials, it is unlikely that activated corticocortical axons would be able to drive other neurons that would then activate mGluRs on the recorded cell. Also, and perhaps more importantly, what is of particular interest is that in cells exhibiting Class 2 responses, we were able to activate mGluRs, whereas we were unable to do so in cells exhibiting Class 1B responses. What is central to our findings is either the presence or absence of an mGluR response following afferent stimulation, but we conclude that the mGluR responses seen here were indeed monosynaptically evoked from thalamus.

Neurons with Group I mGluR responses outnumbered those with Group II mGluR responses (37 vs. 14, with 5 mixed; $P <$

0.001, χ^2 test) with no significant laminar pattern to this difference. To determine if the mGluR responses were plausibly presynaptically or postsynaptically activated, we performed the following control on a subset of 8 cells (2 from layer 5a and 6 from layer 6) that exhibited Class 2 responses. We demonstrated that, with synaptic transmission blocked by a bathing solution of high-Mg²⁺/low-Ca²⁺ and iGluR antagonists, each of these cells responded to application of the general mGluR agonist, ACPD, with a response profile similar to that seen previously after electrical activation of A1 inputs in normal bathing solution.

Figure 4 provides evidence for postsynaptic activation of mGluR1s for one neuron (Fig. 4A–F) and Group II mGluRs for another (Fig. 4G–L). While still in normal ACSF, bath application of ACPD, causes a dramatic and sustained depolarization of the layer 6 A2v neuron (Fig. 4D). Switching to high-Mg²⁺/low-Ca²⁺ ACSF and iGluR antagonists, the neuron continues to respond in the presence of ACPD (Fig. 4E). Note that the response in Figure 4E is smaller than that in Figure 4D, and presumably this is related to the difference in bath Ca²⁺ concentrations. Finally, once the mGluR1 antagonist, Ly367385 is added to the bath, all further responsiveness is gone (Fig. 4F). Figure 4G–L illustrates an analogous experiment showing that a Group II mGluR response is also postsynaptic. Low-frequency electrical

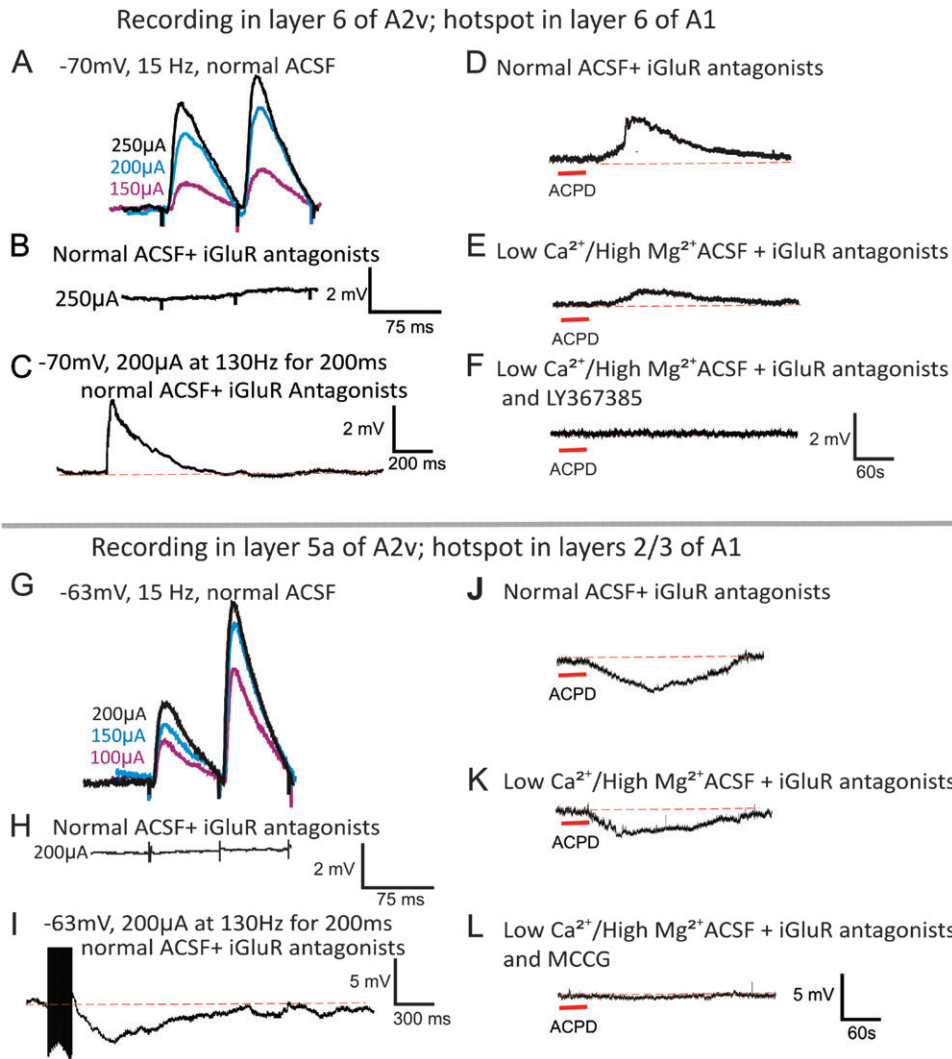


Figure 4. Postsynaptic activation of mGluRs in the A1 to A2v pathway. (A–F) Example showing activation of mGluR1s with paired-pulse facilitation (A), responses to low-frequency stimulation blocked by iGluR antagonists (B), and evidence of mGluR activation (C). With normal ACSF and iGluR antagonists, the addition of ACPD evokes a sustained depolarization (D), which is also seen after a switch to high-Mg²⁺/low-Ca²⁺ ACSF and iGluR antagonists (E). Subsequent addition of mGluR1 antagonist abolishes this response to ACPD (F). (G–L) Example in another neuron showing activation of Group II mGluRs; conventions as in A–F, but in this case the activation of the mGluRs is hyperpolarizing.

stimulation elicits paired-pulse facilitation that is knocked out in the presence of iGluR antagonists. A slow and sustained response is induced by high-frequency electrical stimulation. Note that this stimulation elicits a hyperpolarizing response (Fig. 4G–I). Bath application of ACPD also leads to a long sustained hyperpolarizing response (Fig. 4J). Switching to high-Mg²⁺/low-Ca²⁺ ACSF and iGluR antagonists, the neuron continues to respond with hyperpolarization in the presence ACPD (Fig. 4K). With the addition of MCCG, a Group II mGluR antagonist, to the bath, the cell no longer responds to ACPD (Fig. 4L). Although this approach does not absolutely guarantee that the mGluRs evoked with electrical stimulation are the same as evoked with ACPD when synaptic transmission is blocked, it strongly supports that conclusion (Lee and Sherman 2009a, 2009b).

The population data revealed that both Class 1B and Class 2 responses were activated in a graded fashion, meaning that the evoked EPSP amplitude exhibited a positive monotonic relationship with the amount of current used for stimulation (Fig. 5A). To assess if there was a difference in EPSP amplitude

between Classes, we examined the amplitude of the first EPSP elicited from stimulation at 100 μ A, a level chosen because it was a relatively low intensity that evoked EPSPs in the vast majority of cases. We plotted the ratio of the amplitude of the second EPSP to that of the first EPSP versus the amplitude of the initial EPSP. Figure 5B shows that the first evoked EPSPs for Class 1B responses were significantly larger than those of Class 2 responses ($P < 0.001$ on a Mann–Whitney U -test). Class 1B responses consistently had a paired-pulse ratio, or an EPSP2/EPSP1 amplitude ratio, less than 1 (ratio: 0.61 ± 0.21) and a lack of an mGluR component. For Class 2 responsive cells, the ratio was always greater than 1 (ratio: 1.89 ± 0.84) accompanied by the presence of an mGluR component. Figure 5B also shows for both Classes the relationship among these variables, with the mGluR variable represented by the absolute deflection from baseline in mV in the response to a tetanus stimulation train 200–400 ms after the train finished. Note that this graph shows clear clustering, justifying the classification of Classes 1B and 2 used here. Regarding the relationship between the first EPSP amplitude and the paired-pulse ratio, the total population

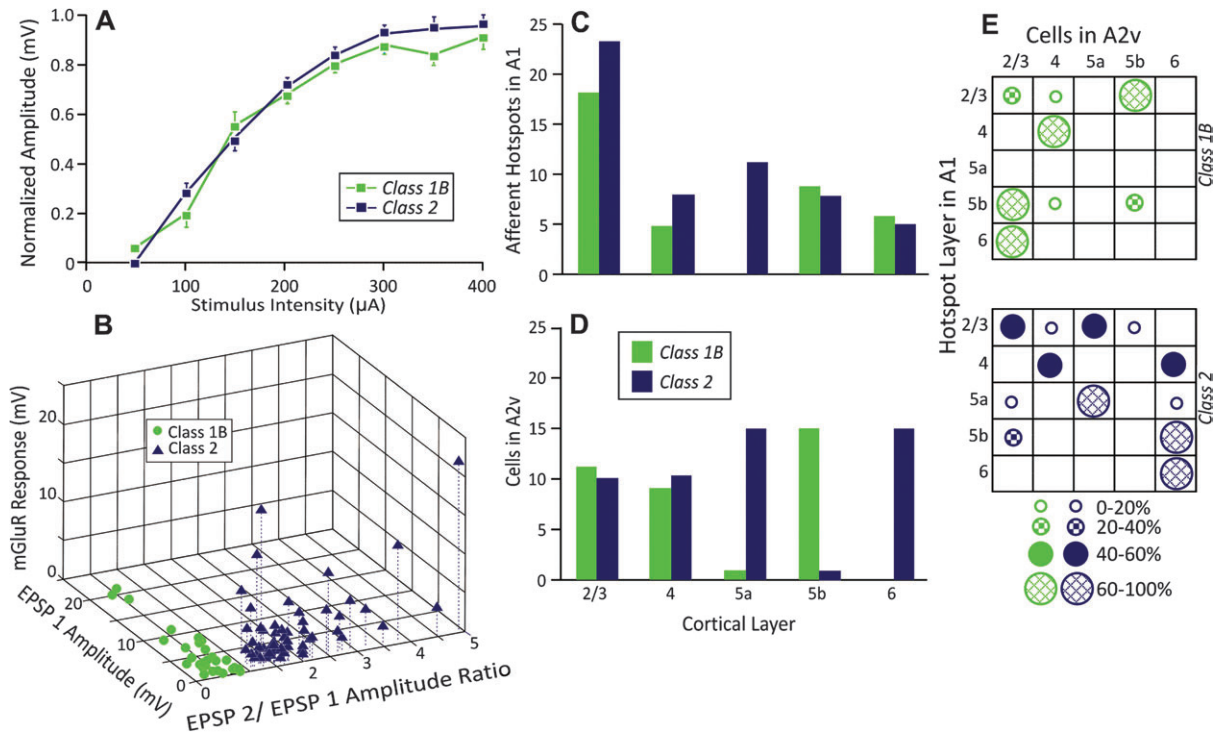


Figure 5. Properties of Class 1B and Class 2 responses. (A) Averaged normalized first EPSP amplitude plotted against stimulus intensity. (B): 3D scatter plot showing relationship among amplitude of first EPSP at threshold activation, the ratio of amplitude of the second to first EPSP at average minimal stimulus intensity, and the mGluR response (see text for description). (C) Laminar origins in A1 of inputs that activated cells in A2v. (D) Laminar location of cells in A2v receiving inputs from A1. (E) Matrix showing A1 laminar origins of inputs to A2v against the laminar locations of postsynaptic cells recorded in A2v. The symbol in each cell indicates the percentage of neurons recorded in the indicated layer of A1 that received input from the indicated layer of A2v.

showed a significant correlation for these variables ($r = -0.403$; $P < 0.0001$), as did cells with Class 2 responses ($r = -0.297$, $P = 0.0291$), but the cells with Class 1B responses showed no such correlation ($r = -0.063$, $P < 0.731$ on a Pearson correlation test for all correlation measurements).

Laminar Relationships

For each patched cell, special attention was paid to its laminar location within A2v and the laminar location of its inputs from A1. Figure 5C shows the laminar location of A1 hotspots, indicating that the plurality emanated from layers 2/3, with smaller contributions from all other layers. All layers gave rise to both types of postsynaptic responses. Figure 5D illustrates the laminar distribution within A2v of cells with each type of response. Class 1B and Class 2 responses are found roughly equally among cells in layers 2/3 and 4. In contrast, cells in layers 5a and 6 exhibited almost exclusively Class 2 responses, whereas those in layer 5b exhibited mostly Class 1B responses. This distribution was significantly different among layers (Kruskal-Wallis: $P < 0.0001$). Finally, Figure 5E combined these data, showing matrices of input layer versus layer of recorded cell for both response types.

There were 38 inputs from A1 that induced Class 1B responses in A2v. For the 18 cells with Class 1B inputs that originated in layers 2/3 of A1, 11 synapsed onto layer 5b of A2v. Each of the 5 inputs originating from layer 4 of A1 synapsed onto layer 4 cells in A2v. We found no cells in A2v that received inputs from layer 5a of A1. Of the 9 inputs from layer 5b, 6 contacted cells in layers 2/3. Finally, each of the 6 inputs originating in layer 6 synapsed onto cells in layers 2/3.

There were 55 inputs from A1 that evoked Class 2 responses in A2v. For the 23 cells with Class 2 responses receiving inputs from layers 2/3 of A1, 10 were in layer 5a, 10 in layers 2/3, and few were in layers 4 ($n = 2$) and 5b ($n = 1$). Of the 8 inputs originating in layer 4 of A1, there were equal numbers to layers 4 and 6, and nowhere else in A2v. Of the 11 inputs originating in layer 5a, 7 synapsed onto layer 5a of A2v and 2 each synapsed onto layers 2/3 and 6. Of the 8 inputs originating in 5b, 6 synapsed onto layer 6, with 2 additional inputs synapsing onto layer 2/3. Finally, all 5 inputs originating in layer 6 of A1 synapsed onto layer 6 of A2v.

Dual Input Hotspots

In 6 experiments, photostimulation of A1 revealed 2 separate hotspots for a recorded cell in A2v. For these cases, we placed stimulating electrodes on each hotspot. In our sample, 4 cells received separate A1 inputs from layers 2/3 and 5b and the other 2 cells from layers 2/3 and 5a. Figure 6A-C shows an example of a cell patched in layers 2/3 receiving Class 2 responses from both layers 5a and 2/3. However, a difference between the 2 inputs was noted such that there was activation of an mGluR1 component for the 5a input and both mGluR1 and mGluR5 components for the layers 2/3 input. Figure 6D-F illustrates another example, in this case a cell recorded in layer 5b that received a Class 2 input from layers 2/3 and a Class 1B input from layer 5b. These examples, while too few in number to generalize, nonetheless show that the variation we see in postsynaptic responses are not dictated solely by the postsynaptic cell.

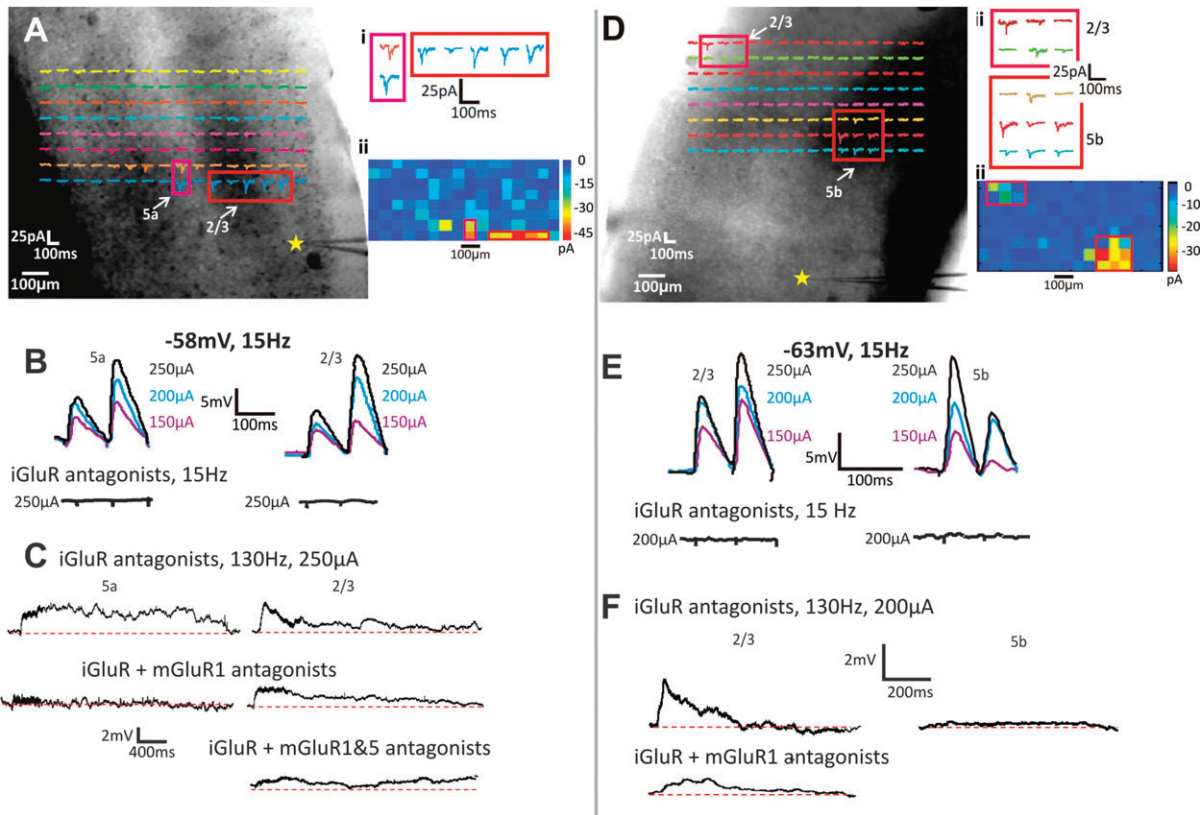


Figure 6. Examples of cells in A2v with inputs from different regions of A1. Conventions as in Figure 3. (A–C) Cell recorded in layer 2/3 with inputs from layers 5a (left traces of B, C) and 2/3 (right traces of B, C). Both input regions produced Class 2 responses, but layer 5a activation involved only mGluR1s, whereas layer 2/3 activation also involved mGluR5s (C). (D–F) Cell recorded in layer 5b with inputs from layers 2/3 (left traces of E, F) and 5b (right traces of E, F). Activation from layers 2/3 produced a Class 2 response and from 5b, a Class 1B response (E, F).

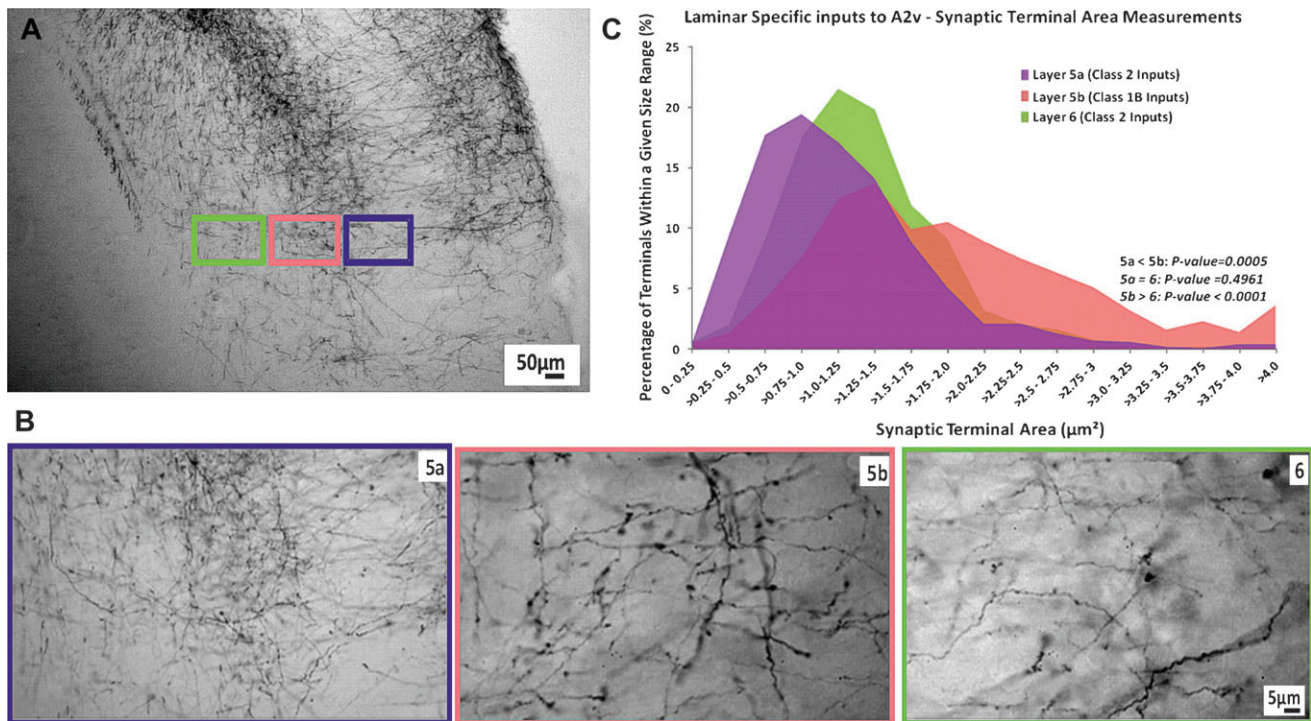


Figure 7. Terminal sizes in A2v from labeling with BDA of inputs from A1. (A) Low-power photomicrograph showing examples of terminal fields in A2v. (B) Higher power views shown of layer 5a (purple box), layer 5b (salmon box), and layer 6 (green box). (C) Size distribution of terminals in layers 5a, 5b, and 6; 1000 terminals were measured from each of the 3 layers.

Anatomical Correlates

To examine the morphology of synaptic terminals projecting from A1 to A2v, tracer injections were made unilaterally into A1. The area of a selected population of labeled synaptic terminals was determined in all layers of A2v. Figure 7*A* shows examples of these terminal fields. We paid particular attention to layers 5a, 5b, and 6, to look for correlations with the response Classes described above, because, as Figure 5*D* shows, layers 5a and 6 receive almost only Class 2 input, whereas layer 5b receives almost only Class 1B input, and other layers received a more equal mix of both types of input. Thus, Figure 7*B* details the size distribution of terminals originating in A1 that terminated in layers 5a, 5b, and 6 of A2v. On average, layers 5a and 6 had smaller terminals than layer 5b (layer 5a, $1.15 \pm 0.68 \mu\text{m}^2$; layer 6, $1.3 \pm 0.51 \mu\text{m}^2$; layer 5b, $1.93 \pm 1.02 \mu\text{m}^2$). The small size differences were not statistically significant for layers 5a and 6 ($P > 0.1$). However, terminals in layer 5b were larger than those in either layer 5a or layer 6 ($P < 0.001$ on Mann-Whitney *U*-tests). Thus, in A2v, layer 5b had Class 1B responsive cells and inputs with larger terminals, whereas layers 5a and 6 had Class 2 responsive cells and inputs with smaller terminals. These terminal size measurements are consistent with previous anatomical data, which demonstrate a wide range of terminal sizes from small to large for afferents with Class 1B properties (Sur et al. 1987; Van Horn and Sherman 2004; Llano and Sherman 2008).

A caveat to these measurements is the possibility that some of the label represents retrograde filling of axons from A2 that produce local terminal fields. We cannot rule out an undefined

number of labeled boutons that originated from A2 and not A1, but we assume that the number of such retrogradely labeled boutons was a relatively small and would serve only to reduce the correlations seen with the physiology. The same caveat applies to the analogous experiment described below in labeling boutons in A1 from injections into A2.

The A2v to A1 Pathway

In the A2v to A1 pathway, whole-cell recordings were obtained from 72 neurons in layers 2/3, 4, 5a, 5b, and 6 of A1, in response to stimulation of A2v. These cells had resting membrane potentials of $-62.4 \pm 3.47 \text{ mV}$ and input resistances of $368.7 \pm 128.2 \text{ M}\Omega$.

Glutamatergic Response Classes

We noted 2 different response profiles, identical to the Class 1B and Class 2 responses exhibited in the A1 to A2v pathway. Figure 8*A–D* shows an example of a Class 1B response for a cell recorded in layer 5b of A1 and activated from layer 5b of A2v (Fig. 8*A*). That is, layer 5b stimulation elicits a large, depressing EPSP with no mGluR component (Fig. 8*D*). The other response pattern we saw, Class 2, is illustrated in Figure 8*E–H* for a cell recorded in layer 5a of A1 and stimulated in layer 5b of A2v (Fig. 8*E*). Here, with iGluRs blocked, layer 5b stimulation evokes a small, facilitating EPSP with an mGluR1 component (Fig. 8*H*). Evidence of postsynaptic activation of this pathway was also verified using the previously described methods involving a low- Ca^{2+} /high- Mg^{2+} bathing solution and can be seen in Figure 9.

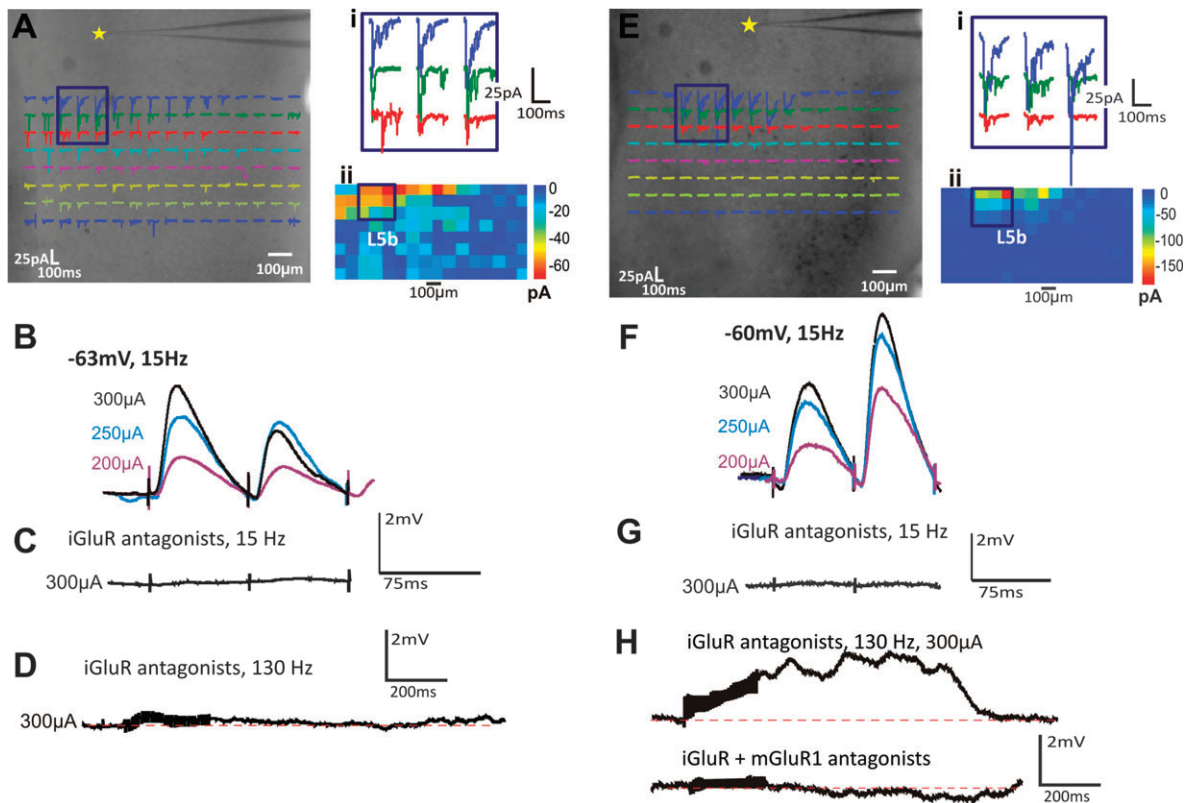


Figure 8. Response examples. Conventions as in Figure 3. (*A–D*) Class 1B response for cell in layer 5b of A1 (star in *A*) with activation hotspot in layer 5b of A2v. Responses enlarged in *A*, and in false color in *A*_{ii}. Electrical stimulation of hotspot shows paired-pulse depression (*B*) with responses blocked by iGluR antagonists (*C*) even at high stimulation rates (*D*). (*E–H*) Class 2 response for cell recorded in layer 5a of A1. Here, we see paired-pulse facilitation (*F*) and depolarizing mGluR activation (*H*); the depolarizing component is blocked by an mGluR1 antagonist (bottom trace).

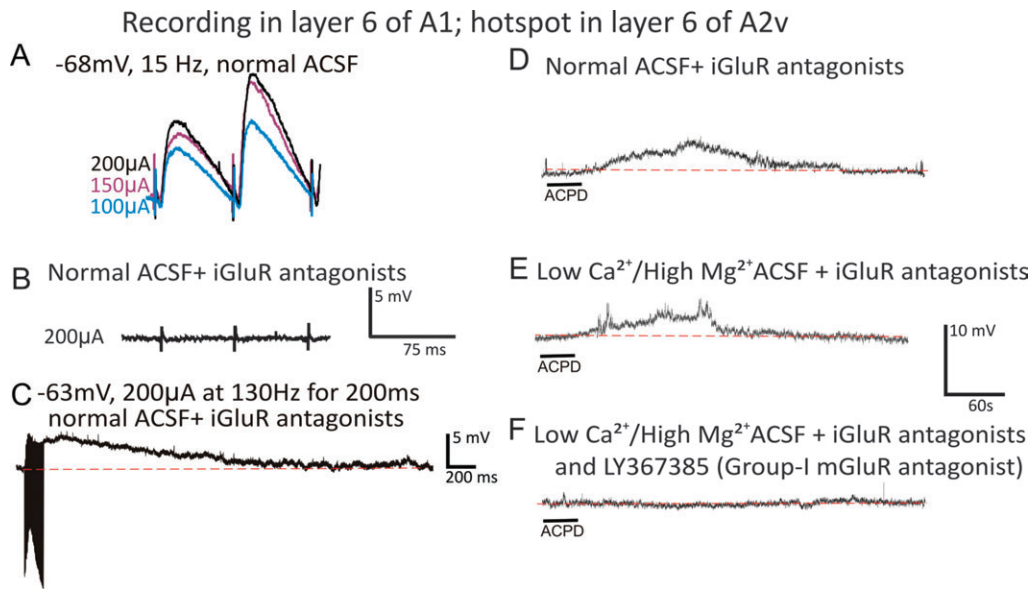


Figure 9. Postsynaptic action of an mGluR response in the A2v to A1 pathway. Conventions as in Figure 4. (A) Paired-pulse facilitation induced by low-frequency stimulation (15 Hz). (B) All responsiveness is knocked out in the presence of iGluR antagonists. (C) High-frequency (130 Hz) stimulation with iGluR antagonists elicits a sustained depolarized response. (D) In normal ACSF, the addition of ACPD pharmacologically induces a sustained depolarized response. (E) Switching to high-Mg²⁺/low-Ca²⁺ ACSF and iGluR antagonists, the neuron depolarizes in response to ACPD application. (F) This response to ACPD is eliminated with the addition of an mGluR1 antagonist.

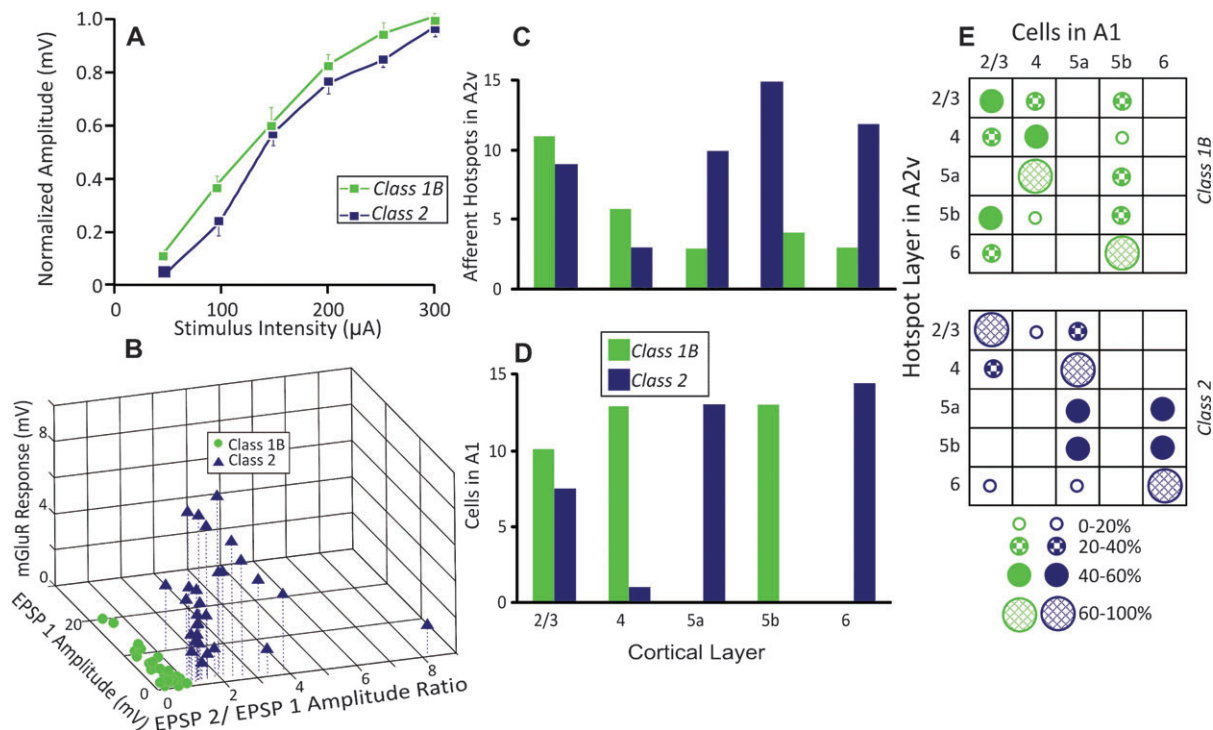


Figure 10. Properties of Class 1B and Class 2 responses. Conventions as in Figure 7. (A) Averaged normalized first EPSP amplitude plotted against stimulus intensity. (B) 3D scatter plot showing relationship among amplitude of first EPSP at threshold activation, the ratio of amplitude of the second to first EPSP at average minimal stimulus intensity, and the mGluR response (see text for description). (C) Laminar origins in A2v of inputs that activated cells in A2v. (D) Laminar location of cells in A1 receiving inputs from A2v. (E) Matrix showing A2v laminar origins of inputs to A1 against the laminar locations of postsynaptic cells recorded in A1.

The population data for the A2v to A1 pathway revealed that both Class 1B and Class 2 responses were also activated in a graded fashion (Fig. 10A). Figure 10B shows that the first evoked EPSP for Class 1B responses were significantly larger than those of Class 2 responses ($P < 0.001$ on a Mann-Whitney U -test). Class 1B responses consistently had a paired-pulse ratio,

or an EPSP2/EPSP1 amplitude ratio, less than 1 (ratio: 0.66 ± 0.14) and a lack of an mGluR component. For Class 2 responsive cells, the ratio was always greater than 1 (ratio: 1.77 ± 0.44) accompanied by the presence of an mGluR component. Figure 10B also shows, as does Figure 5B, clear clustering between Classes 1B and 2 among the variables of first EPSP amplitude,

paired-pulse ratio, and mGluR response. Finally, the total population showed a significant correlation between first EPSP amplitude and paired-pulse ratio ($r = -0.342$; $P = 0.0066$). Significant correlation was not seen amongst the individual population of cells with Class 1B responses ($r = -0.119$, $P = 0.516$) nor the cells with Class 2 responses ($r = -0.244$, $P = 0.194$).

Laminar Relationships

Figure 10C shows the laminar location of A2v hotspots, indicating that all layers gave rise to both types of postsynaptic response. Almost half of the inputs that induced Class 1B responses emanated from layers 5b, with smaller contributions from all other layers. Figure 10D illustrates the laminar distribution within A1 of cells with each type of response.

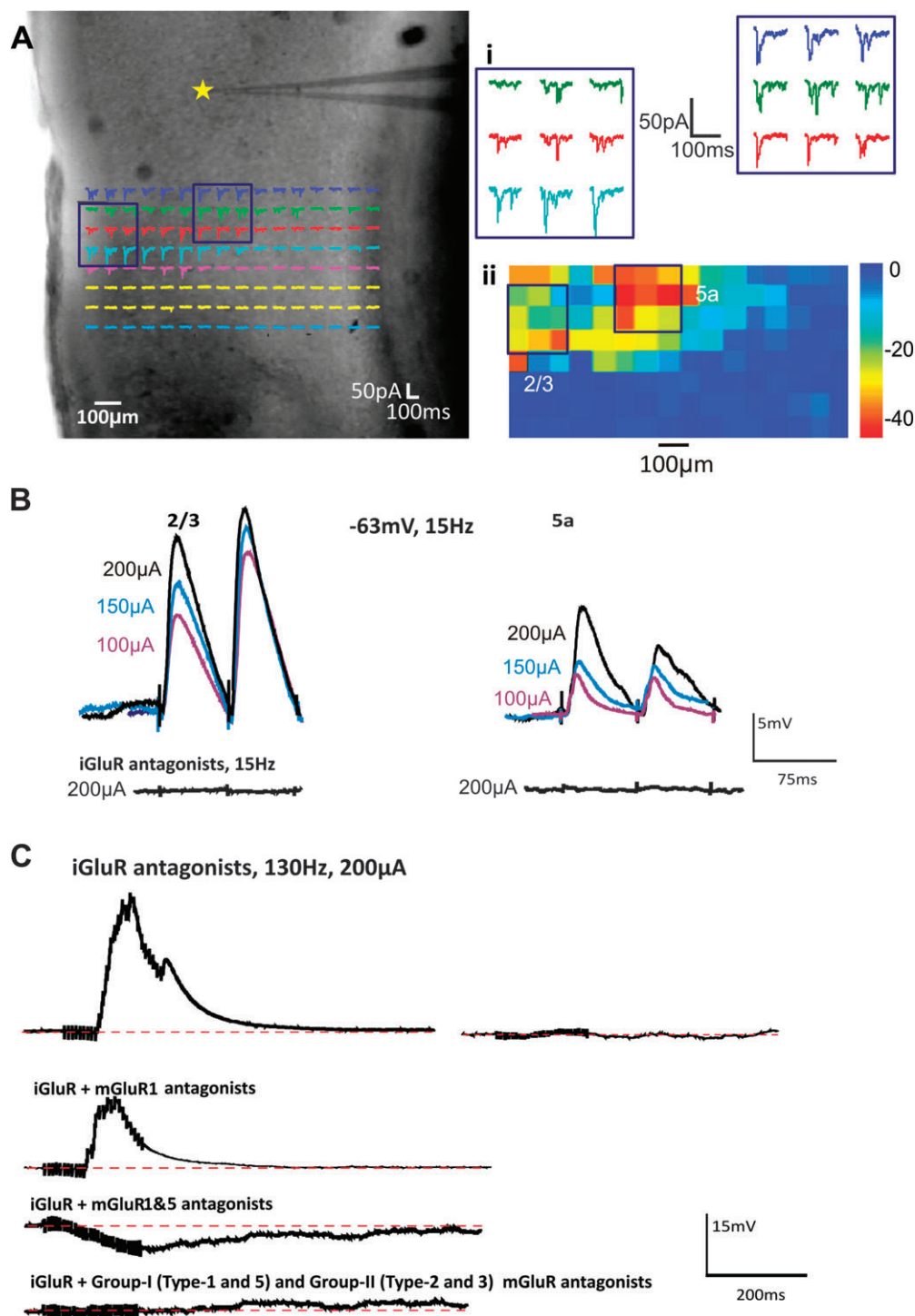


Figure 11. Examples of cell in A1 with inputs from different regions of A2v. Conventions as in Figure 3. (A–C) Cell recorded in layer 4 with inputs from layers 2/3 (left traces of B,C) and 5a (right traces of B,C). Stimulation of layers 2/3 elicits a Class 2 response, while stimulation of layer 5a elicits a Class 1B response (C–D). In the presence of the mGluR1 antagonist, stimulation of layers 2/3 continued to produce a sustained excitatory response that was reduced in amplitude. The addition of an mGluR5 antagonist eliminated the depolarizing response, revealing one that was hyperpolarizing. The final addition of MCGG, a Group II mGluR antagonist, eliminated all responses (C).

Class 1B and Class 2 responses are both found among cells in layer 2/3 (although dominated by Class 1B responses). Similar to the A1 to A2v pathway, cells in layers 5a and 6 exhibited Class 2 responses, whereas those in layers 4 and 5b were limited to Class 1B responses. This distribution was significantly different among layers (Kruskal-Wallis: $P < 0.0001$). Finally, Figure 10E combined these data, showing matrices of input layer versus layer of recorded cell for both response types.

There were 38 inputs from A2v that evoked Class 1B responses in A1. For the 11 inputs that originated in layers 2/3 of A2v, 5 synapsed onto layer 2/3 of A2v, with 3 each synapsing onto layer 4 and layer 5b. Of the 6 Class 1B inputs originating from layer 4 of A2v, 3 synapsed onto layer 4 cells in A1. Other inputs synapsed onto layers 2/3 ($n = 2$) and 5b ($n = 1$). Very few cells in A1 received inputs from layer 5a of A2v ($n = 2$ synapsed onto layer 4 and $n = 1$ onto layer 5b). Of the 15 inputs from layer 5b, 8 contacted cells in layers 2/3, 2 contacted cells in layers 4 and, 5 contacted cells in layers 5b. Finally, of the 3 inputs originating in layer 6 of A2v, 1 synapsed onto cells in layers 2/3 and 2 synapsed onto layer 5b.

Likewise, there were 38 inputs from A2v that induced Class 2 responses in A1. For the 9 cells receiving inputs from layers 2/3 of A2v, 6 were in layer 2/3, 1 in layer 4, and 2 were in layer 5a. For the 3 inputs originating in layer 4, 1 was in 2/3 and 2 were in layer 5a. The 10 inputs originating in layer 5a synapsed equally onto layer 5a and layer 6. The 4 inputs originating in layer 5b synapsed equally onto layer 5a and layer 6. Finally, out of the 12 inputs originating in layer 6, 8 synapsed onto layer 6 of A1, with smaller numbers synapsing on layers 2/3 ($n = 2$) and 5a ($n = 2$).

Dual Input Hotspots

As described above for inputs from A1 to A2v, photostimulation of A2v occasionally revealed 2 hotspots, this being the case for 4 cells recorded in A1 from either layers 2/3 and 5b ($n = 2$) or 2/3 and 5a

($n = 2$). In each instance, a stimulating electrode was placed on each excitation site. Figure 11 shows an example of a cell recorded in layer 4 of A1 that is activated with a Class 2 response from layer 2/3 of A2 and a Class 1B response from layer 5a.

Anatomical Correlates

We repeated the experiment described above to study the morphological correlation of synaptic terminal sizes, in this case, for the A2v to A1 pathway. Bulk biocytin or BDA injections were made unilaterally into A2v (Fig. 12A); tissue processing and terminal measurements were done as described above. Figure 12B shows examples of these terminal fields. On average, layers 5a and 6, which receive only Class 2 inputs, have significantly smaller terminals than layers 4 and 5b, which receive only Class 1B inputs ($5a = 0.83 \pm 0.35 \mu\text{m}^2$, $6 = 1.2 \pm 0.36 \mu\text{m}^2$; $4 = 1.82 \pm 0.25 \mu\text{m}^2$, $5b = 2.53 \pm 0.29 \mu\text{m}^2$; Fig. 12C). We limited our analysis to layers known to receive predominantly Class 1B or Class 2 inputs. Note that the size differences were not statistically significant for layers 5a and 6 nor were they for layers 4 and 5b ($P > 0.1$ on Mann-Whitney U -tests). However, terminals in layers 4 and 5b were larger than those in layers 5a and 6 ($P < 0.001$ on Mann-Whitney U -tests).

Notes on Both Pathways

For laser uncaging experiments, the distance from the recorded cell to the edge of the afferent footprint ranged from 250 to 450 μm (mean: $287.8 \pm 66.47 \mu\text{m}$) in both pathways. It should be noted that there was no significant correlation with that distance and the prevalence of Class 1B or Class 2 response types (overall population of Class 1B and Class 2 responses: $r = -0.277$; from A1 to A2v: $r = -0.379$; from A2v to A1: $r = -0.229$). This held true for that distance and the prevalence of Class 2 glutamatergic metabotropic response type (overall population of Class 2 responses: $r = -0.167$; from A1 to A2v: $r = -0.352$; from

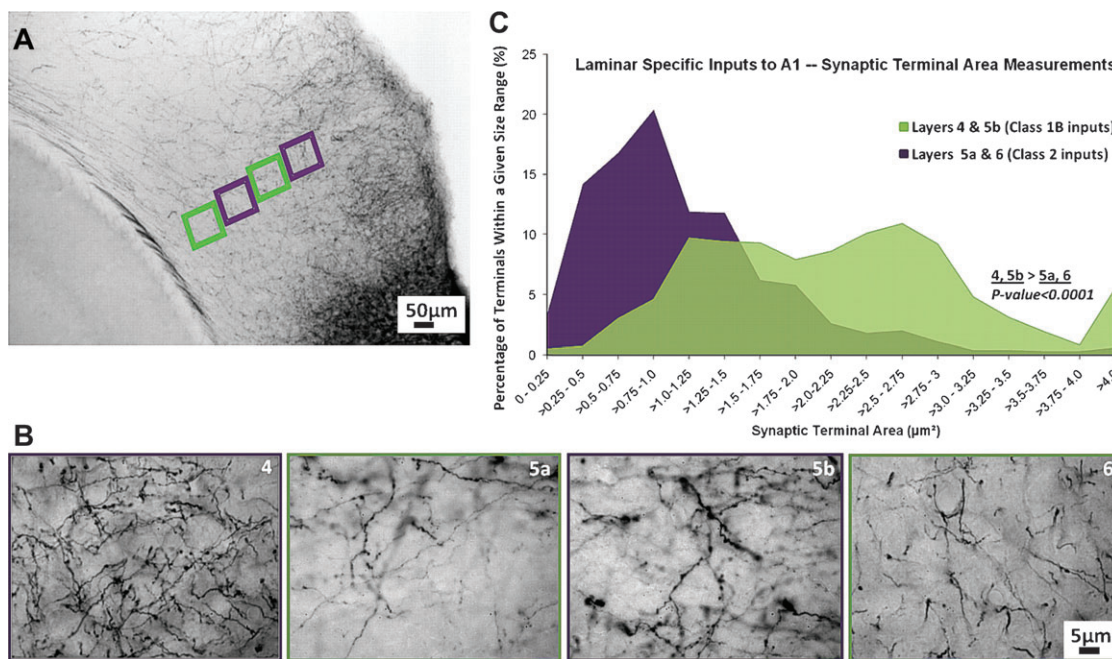


Figure 12. Measurement of laminar-specific terminal size. (A) Lower power photomicrograph of A1 terminal fields after a bulk BDA injection into A2v. (B) Higher power photographs of view are shown at the upper left following the color codes of the rectangles in A and indicating laminar location. (C) Size distributions of terminals pooled across layers 4 and 5b versus layers 5a and 6; 1000 terminals were sampled for each group.

A2v to A1: $r < -0.001$). Finally, although synaptic connections are changing during this stage of neural development and ages in mice, there was no significant correlation with the age of the mouse (as noted in Materials and Methods, 12–19 days postnatal) and the prevalence of Class 1B or Class 2 response types (overall population of Class 1B and Class 2 responses: $r = -0.142$; from A1 to A2v: $r = -0.048$; from A2v to A1: $r = -0.139$). The same can be said for the age and the prevalence of Class 2 glutamatergic metabotropic response type (overall population of Class 2 responses: $r = -0.202$; from A1 to A2v: $r = -0.097$; from A2v to A1: $r = -0.286$).

Discussion

All glutamatergic corticocortical synapses in this study, between A1 and A2v, can be broken down into 2 groups. The first, Class 1B, exhibit large EPSPs with paired-pulse depression, are limited to an iGluR component, and have larger synaptic terminals. The other, Class 2, exhibit small EPSPs with paired-pulse facilitation, iGluR plus mGluR components, and have smaller synaptic terminals. Both response types show a graded activation pattern. It is remarkable that only these 2 Classes were found; we emphasize that it was not our goal to shoehorn glutamatergic inputs into these Classes. We also emphasize here that our goal here was to use techniques applied previously to classify glutamatergic inputs (Reichova and Sherman 2004; Lee and Sherman 2008, 2010; Petrof and Sherman 2009) rather than make an attempt to explore possible mechanisms underlying various differences between Class 1B and Class 2 inputs.

Relationship of Classes 1B and 2 to Drivers and Modulators

Interestingly, the synaptic properties of these Class 1B and Class 2 inputs are nearly identical to those exhibited in the retinogeniculate pathway and various thalamocortical and corticothalamic pathways (Sherman and Guillery 1996, 1998; Reichova and Sherman 2004; Lee and Sherman 2008; 2009a, 2009b; Petrof and Sherman 2009; Viaene et al. 2011). In these pathways, the glutamatergic inputs evoking Class 1B-like responses were called “drivers,” and those evoking Class 2-like responses, “modulators.” An example of a driver input is the retinal input to the lateral geniculate nucleus, and as such, drivers are thought to represent the main information route. An example of a modulator is the feedback corticothalamic input from layer 6, which serves in the LGN mainly to modulate retinogeniculate transmission (for further details, see Sherman and Guillery 1998, 2006). These similarities in classification include differences in terminal size, amplitude of EPSPs, paired-pulse effects, and presence or absence of an mGluR response component.

The one exception to the above is that our Class 1B responses were activated in a graded manner (Figs 5A and 10A), whereas previously described driver inputs were activated in an all-or-none fashion. An all-or-none pattern implies relatively little convergence, and this is consistent with what is known for the retinogeniculate driver pathway (Cleland et al. 1971; Sherman and Guillery 1996, 1998; Usrey et al. 1999; Reichova and Sherman 2004). There is also relatively little convergence in thalamocortical input (Reid and Alonso 1995; Gil and Amitai 1996; Miller et al. 2001), another driver pathway. However, one might expect more convergence in

intracortical pathways due to the more complex computational algorithms expected for cortex. That is, unlike thalamic circuitry for which little receptive field elaboration is seen in driver input to relay cells—for instance, retinal receptive fields are similar to those of their target relay cells—receptive fields in cortex seem to be elaborated as synaptic hierarchies are traversed, and this suggests more convergence of driver inputs. Thus, we tentatively conclude that this graded property in cortex is not inconsistent with driver function. Nonetheless, we choose to note the difference in the graded versus all-or-none response profile by referring to the former (the type seen here) as “Class 1B”), and the latter as “Class 1A.”

With the above caveat, we conclude that Class 1B inputs in this study are the same type as previously described driver inputs and Class 2 inputs, modulator inputs, meaning the classification of glutamatergic inputs first defined for thalamic circuits may be extended to cortex. The whole idea of considering that glutamatergic (and other) pathways might be classified into different functional types seems not yet to have taken much hold. Such classification has always been a key early step in understanding the brain, examples being the classification of neuronal types in retina and cortex. We argue for a similar benefit from classification of pathways, especially glutamatergic ones, to better understand circuits.

We have chosen Class 1B and Class 2 terminology instead of the more provocative driver/modulator terms, because, while a reasonable case can be made that driver (Class 1B) inputs to thalamus provide the main information to be relayed and while Class 2 (modulator) inputs serve mainly to modulate transmission of driver inputs (Sherman and Guillery 1998, 2006), function is less clear for these glutamatergic inputs in the more complex circuitry of cortex. Nonetheless, it seems reasonable to speculate regarding the functional correlates of Class 1B and Class 2 inputs.

Class 1B inputs have, on average, large synaptic terminals associated with large EPSPs; the paired-pulse depression indicates increased probability of transmitter release (Dobrunz and Stevens 1997), and this depression may dynamically regulate neuronal sensitivity during rapid changes in sensory input (Chung et al. 2002). The evoked EPSPs are transient, meaning that an afferent action potential can be represented postsynaptically by a single EPSP up to fairly high afferent firing rates, and thus high rates of temporal information can be faithfully transmitted via this pathway. These are all properties commensurate with a main afferent information source, basically similar to the function proposed for driver input to thalamus (Sherman and Guillery 1996, 1998; Reichova and Sherman 2004).

Class 2 inputs have small terminals that provide small EPSPs, and the paired-pulse facilitation associated with them suggests a low probability of transmitter release (Dobrunz and Stevens 1997). Whereas it is plausible that the iGluR responses evoked by Class 2 inputs can follow high frequencies faithfully because the facilitation seen would favor later responses in a train, higher firing rates of these inputs would also evoke mGluR responses, leading to postsynaptic potentials lasting from hundreds of milliseconds to seconds (Govindaiah and Cox 2006). Such responses typically outlast the input activity, which would distort temporal properties of any information to be processed. Activation of mGluRs also induce relatively long-term changes in the postsynaptic cell, changes that include overall excitability and control of many time- and voltage-gated

conductances that often have inactivation/deinactivation kinetics requiring hundreds of milliseconds (Huguenard et al. 1994; Sherman and Guillery 2001). For all of these reasons, Class 2 inputs are not well suited to transfer of information but are ideally suited for modulation. Furthermore, many of the Class 2 inputs we described are associated with activation of inhibitory Group II mGluRs. Inhibition in cortex, which plays an integral role in the formation of cortical receptive fields and may be involved in such processes as gain control and synaptic plasticity, had been previously thought of as purely GABAergic (Berman et al. 1992; Renger et al. 2002; Hirsch and Martinez 2006; Huang et al. 2007). We suggest that glutamatergic modulatory inputs can also contribute to these inhibitory functions.

For all of the above reasons, we suggest that Class 1B inputs have driver properties and Class 2 inputs serve a basically modulatory role, as do their counterparts innervating thalamus (Sherman and Guillery 1998, 2006). This means that Class 1B inputs represent a main source of information to their target cells, whereas Class 2 inputs modulate the processing of Class 1B inputs.

In the pathway from A1 to A2v, the majority of inputs are Class 2 (modulator). In the pathway from A2v to A1, most of the inputs are Class 1B (driver). In both directions, there is laminar specificity regarding these Class 1B or Class 2 projections in terms of both layer of origin and layer of target cells. We also found a strong correlation between the laminar specificity of synaptic terminal size and the functional synaptic properties of these pathways. Taken together, including the evidence of different types of glutamatergic input and the large number of Class 2 (modulator) inputs, this challenges current dogma about the nature of corticocortical pathways.

All glutamatergic inputs have until recently been generally viewed as more or less equally contributing to information flow, and there was no sustained attempt to functionally classify these inputs. Our evidence is that such a classification is warranted, and our identification here of different glutamatergic input types may be just the beginning of a proper classification scheme of these pathways. Given the suggested functional differences between Class 1B (driver) and Class 2 (modulator) inputs and the hypothesis that information flow depends on Class 1B pathways, this classification dramatically changes the way that functional circuits will be understood.

Significance of Laminar Patterns

The laminar patterns of connections between A1 and A2v in both directions are hard to interpret functionally in detail, but several provisional conclusions can be offered (refer to Figs 5E and 10E). One is that layer 5b receives predominantly Class 1B (driver) input in both directions. Since this layer is the source of a major corticofugal output to thalamus, brainstem, and even spinal cord targets, this suggests that corticocortical projections can have a major influence on these outputs. Furthermore, since layer 6 is the site of feedback corticothalamic projections, and this layer receives purely Class 2 (modulator) input, this suggests that these corticocortical pathways have a more subtle effect on this corticothalamic circuit. That is, the feedback to layer 6 in A1 can affect the status of thalamic input to A1. Because inputs to layers 2–4 are mixed, these corticocortical pathways can have more complex effects on these layers.

One caveat is worth noting regarding our laminar determination of postsynaptic targets. This determination is

based on the location of cell bodies. However, many of the target cells are pyramidal cells, with apical dendrites extending into upper layers. For these cells, it is possible that some of their inputs seen in this study contacted these dendrites in layers other than that occupied by the cell body. In a functional sense, this may be of little concern, and one may doubt whether distal dendritic locations of synapses would be detected by our methods, but we cannot rule this out.

Comparison with Previous Studies

Felleman and Van Essen (1991) have provided the most influential scheme for laminar patterns of corticocortical connections, in both feedforward and feedback directions, and this provides a template against which to compare our results. Briefly, their proposal for feedforward connections suggests that the main target is layer 4; their feedback connections target mostly layers 2 and 6, and their lateral connections target all layers; the source of all of these pathways is layers 2/3, 5, and/or 6 but not 4. A second general conclusion is that feedforward connections are mainly for passing on information and feedback connections are mostly modulatory. A glance at Figures 5E and 10E shows that our laminar pattern of connections, in both directions, matches none of their templates.

There are several possible reasons for this. One is that we are comparing different systems in different species, since Felleman and Van Essen (1991) based theirs on the visual system of rhesus monkeys. Another possible explanation is that their scheme is based almost entirely on anatomical data. That is, estimates of the strength of corticocortical connections have been based on numbers of neurons or terminal fields stained with retrograde and anterograde tracers (Felleman and Van Essen 1991). Thus the scheme that emerges is based on the implied assumption that connections are of a functional weight determined solely by anatomical numbers. The lateral geniculate nucleus of the cat serves as an example of how anatomical numbers can be misleading. Of the 2 glutamatergic inputs to geniculate relay cells, the functionally dominant one is the retinal input, since it provides the basic receptive field properties, while the input from layer 6 of cortex provides a less clear and less dominant effect on these relay cells (Sherman and Guillery 2006); yet the retinal input accounts for only 5% of the synapses onto geniculate relay cells, whereas the cortical input accounts for 30–40% (Erisir et al. 1998; Van Horn et al. 2000). Likewise, only about 6% of the input to layer 4 cells derives from thalamus (Ahmed et al. 1994), but these inputs are Class 1A (Lee and Sherman 2008) and can effectively drive their target cells in cortex (Tanaka 1983; Usrey and Reid 2000; Swadlow and Gusev 2001; Beierlein and Connors 2002; Llano et al. 2009; Theyel et al. 2010). It seems clear from this example that anatomical numbers can be misleading. Yet, if we are correct that Class 1B inputs are dominant for information transfer, even if we limited our connections to Class 1B inputs, we still see little resemblance of this to the Felleman and Van Essen (1991) scheme. This remains an enigma for further study.

Another generally held assumption about corticocortical pathways is that feedforward connections are mainly for passing on information and feedback connections are mostly modulatory (Rockland and Pandya 1979; Stone et al. 1979; Coogan and Burkhalter 1993; Domenici et al. 1995; Callaway 2004, 2005a, 2005b). Again, a glance at Figures 5B and 10B shows no obvious difference in the Class 1B/2 or driver/

modulator mix in the pathways in both directions between A1 and A2v. As with the apparent discrepancy between our observations and those anticipated based on the Felleman and Van Essen (1991) scheme, we need more data to determine how typical our results may be for such connections.

Conclusions

The main conclusion of these studies is that whether from A1 to A2v or from A2v to A1, these corticocortical inputs induce different response types that are often segregated into laminar and sublaminal patterns. Given the suggested functional differences between Class 1B and Class 2 inputs, and the hypothesis that information flow depends on Class 1B pathways, we may need to reconsider cortical hierarchical schemes on the basis of identifying the subsets of pathways that are driving. The data presented here are merely a first step to understanding the synaptic properties of the projections between cortical areas. This is just the beginning of such an analytic approach, and we need data from more corticocortical pathways to determine its validity.

Funding

National Institutes of Health/National Institute on Deafness and Other Communication Disorders (grant DC008794).

Notes

We thank the following people for their help and technical advice in carrying out all experimental procedures and/or manuscript review (in alphabetical order): Drs Joseph Beatty, Jens Christiansen, David Freedman, Christian Hansel, Nicho Hatsopoulos, Joseph Kimmel, Florian Neubauer, and Iraklis Petrof. We specifically thank Charles Lee for providing Group II mGluR histological samples and Angela Viaene for assistance with figures. *Conflict of Interest*: None declared.

References

Ahmed B, Anderson JC, Douglas RJ, Martin KA, Nelson JC. 1994. Polyeuronal innervation of spiny stellate neurons in cat visual cortex. *J Comp Neurol.* 341:39–49.

Atzori M, Lei S, Evans DI, Kanold PO, Phillips-Tansey E, McIntyre O, McBain CJ. 2001. Differential synaptic processing separates stationary from transient inputs to the auditory cortex. *Nat Neurosci.* 4:1230–1237.

Beck PD, Kaas JH. 1998. Cortical connections of the dorsomedial visual area in new world owl monkeys (*Aotus trivirgatus*) and squirrel monkeys (*Saimiri sciureus*). *J Comp Neurol.* 400:18–34.

Beierlein M, Connors BW. 2002. Short-term dynamics of thalamocortical and intracortical synapses onto layer 6 neurons in neocortex. *J Neurophysiol.* 88:1924–1932.

Berman NJ, Douglas RJ, Martin KA. 1992. GABA-mediated inhibition in the neural networks of visual cortex. *Prog Brain Res.* 90:443–476.

Bhadra N, Lahowetz EA, Foldes ST, Kilgore KL. 2007. Simulation of high-frequency sinusoidal electrical block of mammalian myelinated axons. *J Comput Neurosci.* 22:313–326.

Bravo H, Olavarria J, Torrealba F. 1990. Comparative study of visual inter and intrahemispheric cortico-cortical connections in five native Chilean rodents. *Anat Embryol (Berl).* 181:67–73.

Callaway EM. 2004. Feedforward, feedback and inhibitory connections in primate visual cortex. *Neural Netw.* 17:625–632.

Callaway EM. 2005a. Neural substrates within primary visual cortex for interactions between parallel visual pathways. *Prog Brain Res.* 149:59–64.

Callaway EM. 2005b. Structure and function of parallel pathways in the primate early visual system. *J Physiol.* 566:13–19.

Callaway EM, Katz LC. 1993. Photostimulation using caged glutamate reveals functional circuitry in living brain slices. *Proc Natl Acad Sci U S A.* 90:7661–7665.

Canepari M, Papageorgiou G, Corrie JE, Watkins C, Ogden D. 2001. The conductance underlying the parallel fibre slow EPSP in rat cerebellar Purkinje neurones studied with photolytic release of L-glutamate. *J Physiol.* 533:765–772.

Caviness VS, Jr. 1975. Architectonic map of neocortex of the normal mouse. *J Comp Neurol.* 164:247–263.

Chung S, Li X, Nelson SB. 2002. Short-term depression at thalamocortical synapses contributes to rapid adaptation of cortical sensory responses in vivo. *Neuron.* 34:437–446.

Cleland BG, Dubin MW, Levick WR. 1971. Sustained and transient neurones in the cat's retina and lateral geniculate nucleus. *J Physiol.* 217:473–496.

Colbert CM, Pan E. 2002. Ion channel properties underlying axonal action potential initiation in pyramidal neurons. *Nat Neurosci.* 5:533–538.

Coogan TA, Burkhalter A. 1990. Conserved patterns of cortico-cortical connections define areal hierarchy in rat visual cortex. *Exp Brain Res.* 80:49–53.

Coogan TA, Burkhalter A. 1993. Hierarchical organization of areas in rat visual cortex. *J Neurosci.* 13:3749–3772.

Cruikshank SJ, Killackey HP, Metherate R. 2001. Parvalbumin and calbindin are differentially distributed within primary and secondary subregions of the mouse auditory forebrain. *Neuroscience.* 105:553–569.

Dobrunz LE, Stevens CF. 1997. Heterogeneity of release probability, facilitation, and depletion at central synapses. *Neuron.* 18:995–1008.

Domenici L, Harding GW, Burkhalter A. 1995. Patterns of synaptic activity in forward and feedback pathways within rat visual cortex. *J Neurophysiol.* 74:2649–2664.

Dong H, Shao Z, Nerbonne JM, Burkhalter A. 2004. Differential depression of inhibitory synaptic responses in feedforward and feedback circuits between different areas of mouse visual cortex. *J Comp Neurol.* 475:361–373.

Dudek SM, Friedlander MJ. 1996. Intracellular blockade of inhibitory synaptic responses in visual cortical layer IV neurons. *J Neurophysiol.* 75:2167–2173.

Ehret G. 1997. The auditory cortex. *J Comp Physiol.* 181:547–557.

Erisir A, Van Horn SC, Sherman SM. 1998. Distribution of synapses in the lateral geniculate nucleus of the cat: differences between laminae A and A1 and between relay cells and interneurons. *J Comp Neurol.* 390:247–255.

Felleman DJ, Van Essen DC. 1991. Distributed hierarchical processing in the primate cerebral cortex. *Cereb Cortex.* 1:1–47.

Fleiderovich IA, Binshtok AM, Gutnick MJ. 1998. Functionally distinct NMDA receptors mediate horizontal connectivity within layer 4 of mouse barrel cortex. *Neuron.* 21:1055–1065.

Frick A, Feldmeyer D, Sakmann B. 2007. Postnatal development of synaptic transmission in local networks of L5A pyramidal neurons in rat somatosensory cortex. *J Physiol.* 585:103–116.

Gil Z, Amitai Y. 1996. Properties of convergent thalamocortical and intracortical synaptic potentials in single neurons of neocortex. *J Neurosci.* 16:6567–6578.

Gilbert CD, Wiesel TN. 1989. Columnar specificity of intrinsic horizontal and corticocortical connections in cat visual cortex. *J Neurosci.* 9:2432–2442.

Govindaiah G, Cox CL. 2006. Metabotropic glutamate receptors differentially regulate GABAergic inhibition in thalamus. *J Neurosci.* 26:13443–13453.

Hirsch JA, Martinez LM. 2006. Circuits that build visual cortical receptive fields. *Trends Neurosci.* 29:30–39.

Hishida R, Hoshino K, Kudoh M, Norita M, Shibuki K. 2003. Anisotropic functional connections between the auditory cortex and area 18a in rat cerebral slices. *Neurosci Res.* 46:171–182.

Huang ZJ, Di Cristo G, Ango F. 2007. Development of GABA innervation in the cerebral and cerebellar cortices. *Nat Rev Neurosci.* 8:673–686.

- Huguenard J, McCormick DA, Shepherd GM. 1994. Electrophysiology of the neuron: an interactive tutorial. New York: Oxford University Press.
- Kaas JH. 1996. Theories of visual cortex organization in primates: areas of the third level. *Prog Brain Res*. 112:213-221.
- Kaas JH, Collins CE. 2001. The organization of sensory cortex. *Curr Opin Neurobiol*. 11:498-504.
- Kaskan PM, Kaas JH. 2007. Cortical connections of the middle temporal and the middle temporal crescent visual areas in prosimian galagos (*Otolemur garnetti*). *Anat Rec (Hoboken)*. 290:349-366.
- Lachica EA, Beck PD, Casagrande VA. 1992. Parallel pathways in macaque monkey striate cortex: anatomically defined columns in layer III. *Proc Natl Acad Sci U S A*. 89:3566-3570.
- Lachica EA, Casagrande VA. 1992. Direct W-like geniculate projections to the cytochrome oxidase (CO) blobs in primate visual cortex: axon morphology. *J Comp Neurol*. 319:141-158.
- Lachica EA, Casagrande VA. 1993. The morphology of collicular and retinal axons ending on small relay (W-like) cells of the primate lateral geniculate nucleus. *Vis Neurosci*. 10:403-418.
- Lam YW, Sherman SM. 2005. Mapping by laser photostimulation of connections between the thalamic reticular and ventral posterior lateral nuclei in the rat. *J Neurophysiol*. 94:2472-2483.
- Lee CC, Sherman SM. 2008. Synaptic properties of thalamic and intracortical inputs to layer 4 of the first- and higher-order cortical areas in the auditory and somatosensory systems. *J Neurophysiol*. 100:317-326.
- Lee CC, Sherman SM. 2009a. Glutamatergic inhibition in sensory neocortex. *Cereb Cortex*. 19:2281-2289.
- Lee CC, Sherman SM. 2009b. Modulator property of the intrinsic cortical projection from layer 6 to layer 4. *Front Syst Neurosci*. 3:3.
- Llano DA, Sherman SM. 2008. Evidence for nonreciprocal organization of the mouse auditory thalamocortical-corticothalamic projection systems. *J Comp Neurol*. 507:1209-1227.
- Llano M, Gaznick N, Poeschla EM. 2009. Rapid, controlled and intensive lentiviral vector-based RNAi. *Methods Mol Biol*. 485:257-270.
- Lowenstein PR, Somogyi P. 1991. Synaptic organization of cortico-cortical connections from the primary visual cortex to the posteromedial lateral suprasylvian visual area in the cat. *J Comp Neurol*. 310:253-266.
- Maunsell JH, van Essen DC. 1983. The connections of the middle temporal visual area (MT) and their relationship to a cortical hierarchy in the macaque monkey. *J Neurosci*. 3:2563-2586.
- McCormick DA, von Krosigk M. 1992. Corticothalamic activation modulates thalamic firing through glutamate "metabotropic" receptors. *Proc Natl Acad Sci U S A*. 89:2774-2778.
- McDonald AJ, Mascagni F. 1996. Cortico-cortical and cortico-amygdaloid projections of the rat occipital cortex: a Phaseolus vulgaris leucoagglutinin study. *Neuroscience*. 71:37-54.
- Miller LM, Escabi MA, Read HL, Schreiner CE. 2001. Functional convergence of response properties in the auditory thalamocortical system. *Neuron*. 32:151-160.
- Miller MW. 1985. Cogeneration of retrogradely labeled corticocortical projection and GABA-immunoreactive local circuit neurons in cerebral cortex. *Brain Res*. 355:187-192.
- Pan E, Colbert CM. 2001. Subthreshold inactivation of Na⁺ and K⁺ channels supports activity-dependent enhancement of back-propagating action potentials in hippocampal CA1. *J Neurophysiol*. 85:1013-1016.
- Paxinos G, Franklin KBJ. 2001. The mouse brain in stereotaxic coordinates. San Diego (CA): Academic Press.
- Petrof I, Sherman SM. 2009. Synaptic properties of the mammillary and cortical afferents to the anterodorsal thalamic nucleus in the mouse. *J Neurosci*. 29:7815-7819.
- Porter LL. 1997. Morphological characterization of a cortico-cortical relay in the cat sensorimotor cortex. *Cereb Cortex*. 7:100-109.
- Prieto JJ, Peterson BA, Winer JA. 1994. Laminar distribution and neuronal targets of GABAergic axon terminals in cat primary auditory cortex (AI). *J Comp Neurol*. 344:383-402.
- Reichova I, Sherman SM. 2004. Somatosensory corticothalamic projections: distinguishing drivers from modulators. *J Neurophysiol*. 92:2185-2197.
- Reid RC, Alonso JM. 1995. Specificity of monosynaptic connections from thalamus to visual cortex. *Nature*. 378:281-284.
- Renger JJ, Hartman KN, Tsuchimoto Y, Yokoi M, Nakanishi S, Hensch TK. 2002. Experience-dependent plasticity without long-term depression by type 2 metabotropic glutamate receptors in developing visual cortex. *Proc Natl Acad Sci U S A*. 99:1041-1046.
- Reyes A, Lujan R, Rozov A, Burnashev N, Somogyi P, Sakmann B. 1998. Target-cell-specific facilitation and depression in neocortical circuits. *Nat Neurosci*. 1:279-285.
- Rockland KS, Pandya DN. 1979. Laminar origins and terminations of cortical connections of the occipital lobe in the rhesus monkey. *Brain Res*. 179:3-20.
- Scannell JW, Blakemore C, Young MP. 1995. Analysis of connectivity in the cat cerebral cortex. *J Neurosci*. 15:1463-1483.
- Seltzer B, Pandya DN. 1978. Afferent cortical connections and architectonics of the superior temporal sulcus and surrounding cortex in the rhesus monkey. *Brain Res*. 149:1-24.
- Shao Z, Burkhalter A. 1996. Different balance of excitation and inhibition in forward and feedback circuits of rat visual cortex. *J Neurosci*. 16:7353-7365.
- Shepherd GM, Polgruto TA, Svoboda K. 2003. Circuit analysis of experience-dependent plasticity in the developing rat barrel cortex. *Neuron*. 38:277-289.
- Sherman SM, Guillery RW. 1996. Functional organization of thalamocortical relays. *J Neurophysiol*. 76:1367-1395.
- Sherman SM, Guillery RW. 1998. On the actions that one nerve cell can have on another: distinguishing "drivers" from "modulators". *Proc Natl Acad Sci U S A*. 95:7121-7126.
- Sherman SM, Guillery RW. 2001. Exploring the thalamus. San Diego (CA): Academic Press.
- Sherman SM, Guillery RW. 2006. Exploring the thalamus and its role in cortical function. Cambridge (MA): MIT Press.
- Shipp S, Blanton M, Zeki S. 1998. A visuo-somatomotor pathway through superior parietal cortex in the macaque monkey: cortical connections of areas V6 and V6A. *Eur J Neurosci*. 10:3171-3193.
- Shipp S, Zeki S. 1985. Segregation of pathways leading from area V2 to areas V4 and V5 of macaque monkey visual cortex. *Nature*. 315:322-325.
- Shipp S, Zeki S. 1989. The organization of connections between areas V5 and V1 in macaque monkey visual cortex. *Eur J Neurosci*. 1:309-332.
- Shipp S, Zeki S. 1995. Segregation and convergence of specialised pathways in macaque monkey visual cortex. *J Anat*. 187(Pt 3):547-562.
- Stone J, Dreher B, Leventhal A. 1979. Hierarchical and parallel mechanisms in the organization of visual cortex. *Brain Res*. 180:345-394.
- Sur M, Esguerra M, Garraghty PE, Kritzer MF, Sherman SM. 1987. Morphology of physiologically identified retinogeniculate X- and Y-axons in the cat. *J Neurophysiol*. 58:1-32.
- Swadlow HA, Gusev AG. 2001. The impact of 'bursting' thalamic impulses at a neocortical synapse. *Nat Neurosci*. 4:402-408.
- Tanaka K. 1983. Cross-correlation analysis of geniculostriate neuronal relationships in cats. *J Neurophysiol*. 49:1303-1318.
- Theyel BB, Llano DA, Sherman SM. 2010. The corticothalamic cortical circuit drives higher-order cortex in the mouse. *Nat Neurosci*. 13:84-88.
- Usrey WM, Reid RC. 2000. Visual physiology of the lateral geniculate nucleus in two species of new world monkey: *Saimiri sciureus* and *Aotus trivirgatus*. *J Physiol*. 523(Pt 3):755-769.
- Usrey WM, Reppas JB, Reid RC. 1999. Specificity and strength of retinogeniculate connections. *J Neurophysiol*. 82:3527-3540.
- Van Horn SC, Erisir A, Sherman SM. 2000. Relative distribution of synapses in the A-laminae of the lateral geniculate nucleus of the cat. *J Comp Neurol*. 416:509-520.
- Van Horn SC, Sherman SM. 2004. Differences in projection patterns between large and small corticothalamic terminals. *J Comp Neurol*. 475:406-415.

- Viaene AN, Petrof I, Sherman SM. 2011. Synaptic properties of thalamic input to layers 2/3 and 4 of primary somatosensory and auditory cortices. *J Neurophysiol* 105:279-292.
- Walz W. 2007. Patch-clamp analysis: advanced techniques. Totowa (NJ): Humana Press.
- Wong P, Kaas JH. 2009. An architectonic study of the neocortex of the short-tailed opossum (*Monodelphis domestica*). *Brain Behav Evol* 73:206-228.
- Wu CW, Kaas JH. 2003. Somatosensory cortex of prosimian Galagos: physiological recording, cytoarchitecture, and corticocortical connections of anterior parietal cortex and cortex of the lateral sulcus. *J Comp Neurol* 457:263-292.
- Wu J, Rush A, Rowan MJ, Anwyl R. 2001. NMDA receptor- and metabotropic glutamate receptor-dependent synaptic plasticity induced by high frequency stimulation in the rat dentate gyrus in vitro. *J Physiol* 533:745-755.
- Zeki S. 1980. A direct projection from area V1 to area V3A of rhesus monkey visual cortex. *Proc R Soc Lond B Biol Sci* 207:499-506.
- Zeki S, Shipp S. 1989. Modular connections between areas V2 and V4 of macaque monkey visual cortex. *Eur J Neurosci* 1:494-506.
- Zeki SM. 1970. Interhemispheric connections of prestriate cortex in monkey. *Brain Res* 19:63-75.
- Zeki SM. 1974. Functional organization of a visual area in the posterior bank of the superior temporal sulcus of the rhesus monkey. *J Physiol* 236:549-573.
- Zeki SM. 1976. The projections to the superior temporal sulcus from areas 17 and 18 in the rhesus monkey. *Proc R Soc Lond B Biol Sci* 193:199-207.
- Zeki SM, Sandeman DR. 1976. Combined anatomical and electrophysiological studies on the boundary between the second and third visual areas of rhesus monkey cortex. *Proc R Soc Lond B Biol Sci* 194:555-562.